

Mechanical structure of a spin-1 particle

June-Young Kim,^{1,*} Bao-Dong Sun,^{2,3,4,†} Dongyan Fu,^{5,6,‡} and Hyun-Chul Kim^{7,8,§}

¹*Institut für Theoretische Physik II, Ruhr-Universität Bochum, D-44780 Bochum, Germany*

²*Guangdong Provincial Key Laboratory of Nuclear Science, Institute of Quantum Matter, South China Normal University, Guangzhou 510006, China*

³*Guangdong-Hong Kong Joint Laboratory of Quantum Matter, Southern Nuclear Science Computing Center, South China Normal University, Guangzhou 510006, China*

⁴*Helmholtz Institut für Strahlen- und Kernphysik and Bethe Center for Theoretical Physics, Universität Bonn, D-53115 Bonn, Germany*

⁵*Institute of High Energy Physics, Chinese Academy of Sciences, Beijing 100049, China*

⁶*School of Physical Sciences, University of Chinese Academy of Sciences, Beijing 101408, China*

⁷*Department of Physics, Inha University, Incheon 22212, South Korea*

⁸*School of Physics, Korea Institute for Advanced Study (KIAS), Seoul 02455, South Korea*

(Dated: August 3, 2022)

We investigate the mechanical structure of a spin-1 particle. Introducing three different frameworks, i.e., the three-dimensional (3D) Breit frame, the two-dimensional (2D) Breit frame, and the 2D infinite momentum frame (equivalently the two-dimensional Drell-Yan frame), we scrutinize the 2D and 3D energy-momentum tensor (EMT) distributions in these frames. We first derive the EMT distributions in the 2D Breit frame by performing the Abel transformation. The mass distribution in the 2D Breit frame contains an additional monopole contribution induced geometrically. The pressure distribution in the 2D Breit frame also gets an induced monopole structure. When the Lorentz boost is carried out, the mass distribution in the 2D infinite-momentum frame acquires the induced dipole term. Similarly, we also have the induced dipole contributions to the pressure and shear-force densities. We visualize the 2D mass distributions when the spin-1 particle is polarized along the x - and z -axes. We observe that the 2D mass distribution in the infinite momentum frame exhibit clearly the induced dipole structure when the spin-1 particle is polarized along the x -axis. We also discuss the strong force fields inside a polarized spin-1 particle.

I. INTRODUCTION

The gravitational form factors (GFFs) or energy-momentum tensor (EMT) form factors of a hadron show its mechanical structure (see a recent review [1]). They carry essential information on how its mass and spin are distributed inside, how its stability is acquired, and how the internal force fields are laid out. It implies that the gravitational form factors are equally important as the electromagnetic (EM) form factors. In the modern understanding of hadronic form factors, the gravitational form factors can be understood as the second Mellin moments of the generalized parton distributions (GPDs) [2–6]. The GFFs can also be defined from the matrix element of the EMT operator that comes from the response of the hadron to a variation of the external space-time metric tensor [7, 8]. The two-dimensional (2D) inverse Fourier transforms of the GFFs provide the mass and angular momentum probability distributions in the transverse plane [9–11]. These probability distributions in the transverse plane are called the transverse densities [12]. However, the most intriguing form factor among the GFFs is the D -term (Druck-term) form factor, which furnishes the pressure and shear-force densities. They describe the stability mechanism and mechanics of the hadron. In contrast with spin-0 (pion) and spin-1/2 particles (nucleon), higher multipole form factors emerge for the spin-1 particle, as was shown in the case of the EM form factors of the deuteron and spin-1 particle [13–18]. A similar situation can also be found for the EMT form factors of the Δ isobar [19].

Traditionally, the EM form factors of the nucleon have been used for exhibiting how the charge and magnetization distributions are spatially distributed inside a nucleon in the Breit frame (BF) [20]. Similarly, the nucleon EMT form factors yield the three-dimensional (3D) mass, angular momentum, pressure, and shear-force densities for the nucleon [21, 22]. However, there have been serious criticisms on the 3D densities of the nucleon [9, 11, 12, 20, 23], because the 3D densities can only be probabilistically meaningful for atoms and nuclei, not for the nucleon. The reasoning of the criticism lies in the fact that the intrinsic size of the nucleon (R_N) is comparable to the corresponding

* E-mail: Jun-Young.Kim@ruhr-uni-bochum.de

† E-mail: bao-dong.sun@m.scnu.edu.cn

‡ E-mail: fudongyan@ihep.ac.cn

§ E-mail: hchkim@inha.ac.kr

Compton wavelength [24], $\lambda = \hbar/mc$ ($R_N \sim 4\lambda$), which may bring about relativistic corrections up to 20 %. As expected, the relativistic corrections to the distributions for the deuteron are known to be negligible [13, 14], whereas those to the ρ meson should be rather strong. Thus, it is necessary to resolve this problem for the ρ meson. Choosing the infinite-momentum frame (IMF), one can avoid the relativistic corrections but obtain the 2D transverse densities, which suffer from a deficiency of losing information on the longitudinal direction. As proposed in Refs. [13, 25], however, one can view the 3D densities as the quasi-probabilistic ones defined in phase space, taking them fully relativistically. From this perspective, the 3D distributions in the BF provide the intuitive and physical meaning. Then the Abel transformation allows one to project the 3D densities in the BF to the 2D transverse densities [26–28], which was already introduced in describing deeply virtual Compton scattering [29, 30]. The 2D BF EM distributions for the ρ meson have been studied [16] where a wave packet is applied to the localized ρ -meson state. Note that, very recently, a novel prescription of defining the 3D distribution was studied in Refs. [31, 32].

In Refs. [26, 27], it was shown that the Abel transformation projects the 3D BF distributions onto the 2D IMF densities. The Abel images of the 3D BF distributions without any non-relativistic approximation are exactly identified as the 2D IMF densities that can be obtained from the 2D Fourier transform of the corresponding form factors. To find the Abel images of the 3D distributions in the BF, one should know the hadronic matrix element in the IMF or the expressions for the 2D distributions in the IMF. In Ref. [27], the four different 3D BF EMT distributions are related to the 2D IMF ones and a complete set of the 2D IMF distributions were determined. The 2D IMF distributions for the transversely polarized nucleon can be found by using the obtained Abel images from the 3D BF distributions.

In the meanwhile, Freese and Miller [33] criticized the Abel transformation from the 3D BF distributions to the 2D IMF ones. They argued that the Abel transformation is merely defined as the integral of a spherical symmetric 3D distribution over z -axis. Having performed the integral of the nucleon EMT distributions $T^{00}(\mathbf{r})$ or $T^{ij}(\mathbf{r})$ over z , they obtained the Abel images in the BF. However, this integral merely projects the 3D BF distribution onto the 2D BF one without any relativistic effects. So, their Abel images are different from those defined in Refs. [26, 27]. Knowing this difference is essential to understand the physical implications of the Abel images. Though we have technical difficulties to construct the Abel images in the IMF from the 3D distributions in the BF for higher spin particles such as the ρ meson and Δ isobar, we can formally establish the Abel images in the IMF for these particles [26, 27]. The only trouble arises from the fact that relativistic contributions bring about a number of kernels composed of the Laplacians into the Abel transformation [14]. Depending on the order of the differential equations, we need to provide additional boundary conditions on the distributions so that we can perform the integrals. An easy way to circumvent such complexities is to project 3D BF distributions to 2D BF ones as done in Ref. [33]. Then, we can proceed to the IMF by increasing the z -component of the momentum (P_z) to infinity. In the case of the spin-1 particle, however, the procedure from $P_z = 0$ to $P_z = \infty$ is very complicated as shown in Ref. [14]. Nevertheless, we want to emphasize the following point: in Ref. [28] it was explicitly shown that by introducing the kernel for relativistic effects, the 2D IMF transverse charge densities of both the proton and neutron were derived from the nonrelativistic charge and magnetization distributions in 3D space. The results for the transverse charge densities are exactly the same as those obtained in Ref. [12]. Thus, the IMF Abel images directly obtained from the 3D distributions [26–28] are immune to the criticism raised in Ref. [33].

In the present work, we want to investigate the EMT densities of a spin-1 particle, focusing on the mechanical structure of the GFFs and the corresponding densities of the spin-1 particle instead of describing the GFFs of the spin-1 particle [13, 14, 34] quantitatively. The outline of the current work is given as follows: In the next Section, we define the GFFs of a spin-1 particle in three different frames such as the 3D BF, 2D BF, and 2D IMF. In Section III, we show how to obtain the densities in the three different frames. In Section IV, we formulate the Abel transformation for the EMT densities. In Section V, we introduce a toy model, where the GFFs are parametrized as simple quadrupole types, and derive the 2D EMT densities. We discuss the physical implications of the numerical results and 2D force fields inside a spin-1 particle. In the final section, we summarize the current work and draw conclusions.

II. GRAVITATIONAL FORM FACTORS OF A SPIN-1 PARTICLE

The EMT operator of quantum chromodynamics (QCD) can be derived either by varying the action of QCD under the Poincaré transformation with the symmetrization imposed [35–37] or by taking variation of the QCD action, which is coupled to the weak classical torsionless gravitational background field, with respect to the metric tensor of this curved background field [1, 38]. The total EMT operator consisting of the quark (q) and gluon (g) parts are then written by

$$\hat{T}^{\mu\nu} = \sum_q \hat{T}_q^{\mu\nu} + \hat{T}_g^{\mu\nu}, \quad (1)$$

where the quark and gluon parts are expressed respectively as

$$\begin{aligned}\hat{T}_q^{\mu\nu} &= \frac{1}{4}\bar{\psi}_q \left(-i\overleftarrow{\mathcal{D}}^\mu\gamma^\nu - i\overleftarrow{\mathcal{D}}^\nu\gamma^\mu + i\overrightarrow{\mathcal{D}}^\mu\gamma^\nu + i\overrightarrow{\mathcal{D}}^\nu\gamma^\mu \right) \psi_q - g^{\mu\nu}\bar{\psi}_q \left(-\frac{i}{2}\overleftarrow{\mathcal{D}} + \frac{i}{2}\overrightarrow{\mathcal{D}} - m_q \right) \psi_q, \\ \hat{T}_g^{\mu\nu} &= F^{a,\nu\eta}F^{a,\nu}{}_\eta + \frac{1}{4}g^{\mu\nu}F^{a,\kappa\eta}F^{a,\kappa\eta}.\end{aligned}\quad (2)$$

Here, $\overrightarrow{\mathcal{D}}_\mu = \overrightarrow{\partial}_\mu +igt^a A_\mu^a$ and $\overleftarrow{\mathcal{D}}_\mu = \overleftarrow{\partial}_\mu -igt^a A_\mu^a$ are covariant derivatives. t^a stand for the SU(3) color group generators that satisfy the commutation relations $[t^a, t^b] = if^{abc}t^c$ and are normalized as $\text{tr}(t^a t^b) = \frac{1}{2}\delta^{ab}$. ψ_q is the quark operator with flavor index q and m_q represents the corresponding current quark mass. $F^{a,\mu\eta}$ denotes the gluon field strength expressed as $F_{\mu\nu}^a = \partial_\mu A_\nu^a - \partial_\nu A_\mu^a - gf^{abc}A_\mu^b A_\nu^c$. The total EMT operator is a conserved current: $\partial^\mu \hat{T}_{\mu\nu} = 0$.

The matrix element of the total EMT current operator for a spin-1 particle is parametrized in terms of the six different form factors [39–41]

$$\begin{aligned}\langle p', \lambda' | \hat{T}_{\mu\nu}(0) | p, \lambda \rangle &= \left[2P_\mu P_\nu \left(-\epsilon'^* \cdot \epsilon A_0(t) + \frac{\epsilon'^* \cdot P \epsilon \cdot P}{m^2} A_1(t) \right) \right. \\ &\quad + 2 \left[P_\mu (\epsilon'_\nu{}^* \epsilon \cdot P + \epsilon_\nu \epsilon'^* \cdot P) + P_\nu (\epsilon'_\mu{}^* \epsilon \cdot P + \epsilon_\mu \epsilon'^* \cdot P) \right] J(t) \\ &\quad + \frac{1}{2} (\Delta_\mu \Delta_\nu - \eta_{\mu\nu} \Delta^2) \left(\epsilon'^* \cdot \epsilon D_0(t) + \frac{\epsilon'^* \cdot P \epsilon \cdot P}{m^2} D_1(t) \right) \\ &\quad + \left[\frac{1}{2} (\epsilon_\mu \epsilon'_\nu{}^* + \epsilon'_\mu{}^* \epsilon_\nu) \Delta^2 - (\epsilon'_\mu{}^* \Delta_\nu + \epsilon'_\nu{}^* \Delta_\mu) \epsilon \cdot P \right. \\ &\quad \left. + (\epsilon_\mu \Delta_\nu + \epsilon_\nu \Delta_\mu) \epsilon'^* \cdot P - 4\eta_{\mu\nu} \epsilon'^* \cdot P \epsilon \cdot P \right] E(t) \Big],\end{aligned}\quad (3)$$

where the one-particle state for the spin-1 particle is normalized as $\langle p', \lambda' | p, \lambda \rangle = 2p^0 (2\pi)^3 \delta_{\lambda'\lambda} \delta^{(3)}(\mathbf{p}' - \mathbf{p})$ with the spin polarizations of the initial λ and final λ' states. $P = (p + p')/2$ designates the average of the four-momenta p and p' , and $\Delta = p' - p$ represents the four-momentum transfer with $\Delta^2 = t$. P and Δ are orthogonal each other, i.e., $P \cdot \Delta = 0$. The polarization vectors are defined as $\epsilon'_\mu = \epsilon'_\mu(p', \lambda')$, $\epsilon_\mu = \epsilon_\mu(p, \lambda)$ for simplicity. In this work, we choose canonical spin states (see relevant discussions [25, 42, 43]). It can be obtained by applying the rotationless boost operator to the spin-one polarization vector $e^\mu(0, \lambda) = (0, \hat{\epsilon}_\lambda)$ in the rest frame. The explicit expression of the spin-one vector e^μ in any frame is defined by

$$e^\mu(p, \lambda) = \left(\frac{\mathbf{p} \cdot \hat{\epsilon}_\lambda}{m}, \hat{\epsilon}_\lambda + \frac{\mathbf{p} \cdot \hat{\epsilon}_\lambda}{m(m + p_0)} \mathbf{p} \right) \quad (4)$$

with

$$\hat{\epsilon}_x = (1, 0, 0), \quad \hat{\epsilon}_y = (0, 1, 0), \quad \hat{\epsilon}_z = (0, 0, 1), \quad (5)$$

in the Cartesian basis. $\eta_{\mu\nu}$ is the metric tensor $\eta_{\mu\nu} = \text{diag}(1, -1, -1, -1)$. $A_0(t)$, $A_1(t)$, $J(t)$, $D_0(t)$, $D_1(t)$, and $E(t)$ are the six independent GFFs of the spin-1 particle. Since the total (quark+gluon) current is conserved, we do not consider the non-conserving terms arising from the quark and gluon parts separately (see Ref. [41] for the separate quark and gluon GFFs).

Since the GFFs of a spin-1 particle reveal higher multipole structures, it is useful to define the quadrupole operator \hat{Q}^{ij} . It is defined in terms of the spin operator \hat{S}^i as

$$\hat{Q}^{ij} = \frac{1}{2} \left(\hat{S}^i \hat{S}^j + \hat{S}^j \hat{S}^i - \frac{2}{3} S(S+1) \delta^{ij} \right), \quad (6)$$

where the indices i and j run over 1, 2, and 3. \hat{Q}^{ij} is a symmetric irreducible tensor operator. The components of the spin operators can be expressed in terms of the SU(2) Clebsch-Gordan coefficients $C_{S\sigma'1a}^{S\sigma}$ in the spherical basis

$$\hat{S}_{\sigma'\sigma}^a = \sqrt{S(S+1)} C_{S\sigma'1a}^{S\sigma} \quad \text{with} \quad (a = 0, \pm 1, \quad \sigma, \sigma' = 0, \dots, \pm S). \quad (7)$$

A. Gravitational form factors of the spin-1 particle in the 3D Breite frame

We first examine the matrix element of the EMT operators (3) in the 3D BF. To examine the multipole structure of the GFFs, we need to define the n -rank irreducible Cartesian tensors, which are expressed respectively in coordinate

and momentum spaces

$$Y_n^{i_1 i_2 \dots i_n}(\Omega_r) = \frac{(-1)^n}{(2n-1)!!} r^{n+1} \partial^{i_1} \partial^{i_2} \dots \partial^{i_n} \frac{1}{r}, \quad Y_n^{i_1 i_2 \dots i_n}(\Omega_\Delta) = \frac{(-1)^n}{(2n-1)!!} \Delta^{n+1} \partial^{i_1} \partial^{i_2} \dots \partial^{i_n} \frac{1}{\Delta}, \quad (8)$$

where the first three of $Y_n^{i_1 i_2 \dots i_n}(\Omega_r)$ are explicitly written as

$$Y_0(\Omega_r) = 1, \quad Y_1^i(\Omega_r) = \frac{r^i}{r}, \quad Y_2^{ij}(\Omega_r) = \frac{r^i r^j}{r^2} - \frac{1}{3} \delta^{ij}. \quad (9)$$

In the BF, the four-momenta of the initial and final states are respectively expressed as $p = (p^0, \mathbf{p})$ and $p' = (p^0, -\mathbf{p})$, which yield $\Delta^0 = 0$ and $\mathbf{P} = \mathbf{0}$. Then we consider the matrix element of each component of the EMT current:

$$\begin{aligned} \langle p', \lambda' | \hat{T}^{00}(0) | p, \lambda \rangle &= 2m^2 \mathcal{E}_0(t) \delta_{\lambda' \lambda} + 4m^2 \tau \mathcal{E}_2(t) \hat{Q}^{kl} Y_2^{kl}(\Omega_\Delta), \\ \langle p', \lambda' | \hat{T}^{0i}(0) | p, \lambda \rangle &= 2m^2 \sqrt{\tau} i \epsilon^{ijk} S^k Y_1^k(\Omega_\Delta) \mathcal{J}_1(t), \\ \langle p', \lambda' | \hat{T}^{ij}(0) | p, \lambda \rangle &= 2m^2 \tau \left(Y_2^{ij}(\Omega_\Delta) - \frac{2}{3} \delta^{ij} \right) \mathcal{D}_0(t) \delta_{\lambda' \lambda} + 8\tau^2 m^2 \left(Y_2^{ij}(\Omega_\Delta) - \frac{2}{3} \delta^{ij} \right) Y_2^{kl}(\Omega_\Delta) \hat{Q}^{kl} \mathcal{D}_3(t) \\ &\quad + 4m^2 \tau \left(Y_2^{jk}(\Omega_\Delta) \hat{Q}^{ik} + Y_2^{ik}(\Omega_\Delta) \hat{Q}^{jk} - \frac{1}{3} \hat{Q}^{ij} - \delta^{ij} Y_2^{kl}(\Omega_\Delta) \hat{Q}^{kl} \right) \mathcal{D}_2(t), \end{aligned} \quad (10)$$

where $\tau = -\frac{t}{4m^2}$ and $\hat{Q}_{\lambda\lambda'}^{ij} = \langle \lambda' | \hat{Q}^{ij} | \lambda \rangle$. For brevity, we define $\hat{Q}^{ij} := \hat{Q}_{\lambda\lambda'}^{ij}$, from now on. Examining these expressions for each component of the matrix element, one can easily relate the multipole form factors $\mathcal{E}_0(t)$, $\mathcal{E}_2(t)$, $\mathcal{J}_1(t)$, $\mathcal{D}_0(t)$, $\mathcal{D}_2(t)$, and $\mathcal{D}_3(t)$ to the GFFs in Eq. (3)

$$\begin{aligned} \mathcal{E}_0(t) &= A_0(t) - \frac{1}{3} \tau \left[-5A_0(t) + 3D_0(t) + 4J(t) - 2E(t) + A_1(t) \right] \\ &\quad - \frac{2}{3} \tau^2 \left[-A_0(t) + D_0(t) + 2J(t) - 2E(t) + A_1(t) + \frac{1}{2} D_1(t) \right] - \frac{1}{3} \tau^3 \left[A_1(t) + D_1(t) \right], \\ \mathcal{E}_2(t) &= -A_0(t) + 2J(t) - E(t) + \frac{1}{2} A_1(t) \\ &\quad + \tau \left[-A_0(t) + D_0(t) + 2J(t) - 2E(t) + A_1(t) + \frac{1}{2} D_1(t) \right] \\ &\quad + \frac{1}{2} \tau^2 \left[A_1(t) + D_1(t) \right], \\ \mathcal{J}_1(t) &= J(t) + \tau \left(J(t) - E(t) \right), \\ \mathcal{D}_0(t) &= -D_0(t) + \frac{4}{3} E(t) - \frac{1}{3} \tau \left[2D_0(t) - 2E(t) + D_1(t) \right] - \frac{1}{3} \tau^2 D_1(t), \\ \mathcal{D}_2(t) &= -E(t), \\ \mathcal{D}_3(t) &= \frac{1}{4} \left[2D_0(t) - 2E(t) + D_1(t) \right] + \frac{1}{4} \tau D_1(t). \end{aligned} \quad (11)$$

B. Gravitational form factors of the spin-1 particle in the 2D Breit frame

In Refs. [25, 44], the elastic frame (EF) was introduced to study how the hadronic matrix element undergoes changes under the Lorentz boost. It was shown that this frame naturally interpolates between the 2D BF and 2D IMF for both the nucleon [25] and the deuteron [13]. The EF also allows one to define a quasi-probabilistic distribution for a moving hadron in the Wigner sense. To trace down the origin of both the geometrical and relativistic effects, we scrutinize how the multipole structure of the EMT matrix element emerges in 2D space. If we restrict ourselves to 2D space, we have to define the 2D n -rank irreducible tensors respectively in 2D coordinate and momentum spaces as follows:

$$X_n^{i_1 \dots i_n}(\theta_{x_\perp}) = \frac{(-1)^{n+1}}{(2n-2)!!} x_\perp^n \partial^{i_1} \dots \partial^{i_n} \ln x_\perp, \quad X_n^{i_1 \dots i_n}(\theta_{\Delta_\perp}) = \frac{(-1)^{n+1}}{(2n-2)!!} \Delta_\perp^n \partial^{i_1} \dots \partial^{i_n} \ln \Delta_\perp \quad (12)$$

with $n > 0$ and $i_n = 1, 2$. x_\perp is the radial distance from the center of the 2D plane. The first three of $X_n^{i_1 \dots i_n}(\theta_{x_\perp})$ are given as

$$X_0(\theta_{x_\perp}) := 1, \quad X_1^i(\theta_{x_\perp}) = \frac{x_\perp^i}{x_\perp}, \quad X_2^{ij}(\theta_{x_\perp}) = \frac{x_\perp^i x_\perp^j}{x_\perp^2} - \frac{1}{2} \delta^{ij}. \quad (13)$$

In the EF, the spacelike momentum transfer $\mathbf{\Delta} = (\mathbf{\Delta}_\perp, 0)$ lies in the 2D transverse plane. The frame satisfies the following conditions: $\mathbf{P} = (\mathbf{0}, P_z)$ and $\Delta^0 = 0$. If we take the 2D BF, i.e., $P_z = 0$, the matrix element for each component of $\hat{T}^{\mu\nu}$ is derived as

$$\begin{aligned}
\langle p', \lambda' | \hat{T}^{00}(0) | p, \lambda \rangle &= 2m^2 \mathcal{E}_{(0,1)}(t) \delta_{\sigma'\sigma} + 2m^2 \mathcal{E}_{(0,0)}(t) \delta_{\lambda'3} \delta_{\lambda 3} + 4m^2 \tau \mathcal{E}_2(t) \hat{Q}^{kl} X_2^{kl}(\theta_{\Delta_\perp}), \\
\langle p', \lambda' | \hat{T}^{0i}(0) | p, \lambda \rangle &= 2m^2 \sqrt{\tau} i \epsilon^{3li} \hat{S}_{\lambda'\lambda}^3 X_1^l(\theta_{\Delta_\perp}) \mathcal{J}_1(t), \\
\langle p', \lambda' | \hat{T}^{ij}(0) | p, \lambda \rangle &= 2m^2 \tau \left[\left(\frac{1}{3} \mathcal{D}_2(t) - \frac{1}{2} \mathcal{D}_0(t) \right) \delta_{\sigma'\sigma} + \left(-\frac{2}{3} \mathcal{D}_2(t) - \frac{1}{2} \mathcal{D}_0(t) \right) \delta_{\lambda'3} \delta_{\lambda 3} \right] \delta^{ij} \\
&\quad + 2m^2 \tau X_2^{ij}(\theta_{\Delta_\perp}) \delta_{\lambda'\lambda} \mathcal{D}_0(t) + 4m^2 \tau \left[\hat{Q}^{ik} X_2^{jk}(\theta_{\Delta_\perp}) + \hat{Q}^{jk} X^{ik}(\theta_{\Delta_\perp}) - \hat{Q}^{lm} X_2^{lm}(\theta_{\Delta_\perp}) \delta^{ij} \right] \mathcal{D}_2(t) \\
&\quad + 8m^2 \tau^2 \hat{Q}^{lm} \left(X_2^{lm}(\theta_{\Delta_\perp}) + \frac{1}{2} \delta^{lm} \right) \left(X_2^{ij}(\theta_{\Delta_\perp}) - \frac{1}{2} \delta^{ij} \right) \mathcal{D}_3(t)
\end{aligned} \tag{14}$$

with

$$\mathcal{E}_{(0,0)}(t) = \mathcal{E}_0(t) + \frac{2}{3} \tau \mathcal{E}_2(t), \quad \mathcal{E}_{(0,1)}(t) = \mathcal{E}_0(t) - \frac{1}{3} \tau \mathcal{E}_2(t), \tag{15}$$

where the definition of the multipole form factors is the same as Eq. (11) and the indices run over $i, j = 1, 2$. We use the following short-handed notation $\delta_{\sigma'\sigma} = \delta_{\sigma'\sigma} \delta_{\lambda'\sigma'} \delta_{\lambda\sigma}$ with $\sigma', \sigma = 1, 2$. We want to mention that the 2D multipole form factors exhibit a distinctive feature in contrast to those in the 3D BF. As shown in Eq. (15), the mass form factors in the 2D BF, $\mathcal{E}_{(0,0)}$ and $\mathcal{E}_{(0,1)}$, acquire respectively the positive and negative contributions from the quadrupole mass form factor \mathcal{E}_2 defined in the 3D BF. It originates from the presence of the quadrupole structure and the geometrical difference between the 2D and 3D spaces. This feature has been already observed in the charge distributions of a higher spin particle ($S \geq 1$) such as the ρ meson [14]. We want to emphasize that they do not come from relativistic effects.

C. Gravitational form factors of the spin-1 particle in the infinite-momentum frame

If we take the value of the P_z as infinity in the EF, we arrive naturally at the IMF. Thus, by taking $P_z \rightarrow \infty$, we obtain the matrix element in the IMF:

$$\begin{aligned}
\langle p', \lambda' | \hat{T}^{00}(0) | p, \lambda \rangle &= 2P_z^2 \mathcal{E}_{(0,0)}^{\text{IMF}}(t) \delta_{\lambda'3} \delta_{\lambda 3} + 2P_z^2 \mathcal{E}_{(0,1)}^{\text{IMF}}(t) \delta_{\sigma'\sigma} \\
&\quad + 2P_z^2 \sqrt{\tau} \mathcal{E}_1^{\text{IMF}}(t) i \epsilon^{3jk} \hat{S}_{\lambda'\lambda}^j X_1^k(\theta_{\Delta_\perp}) + 4P_z^2 \tau \mathcal{E}_2^{\text{IMF}}(t) \hat{Q}^{kl} X_2^{kl}(\theta_{\Delta_\perp}), \\
\langle p', \lambda' | \hat{T}_a^{0i}(0) | p, \lambda \rangle &= 2m P_z \sqrt{\tau} i \epsilon^{3li} \hat{S}_{\lambda'\lambda}^3 X_1^l(\theta_{\Delta_\perp}) \mathcal{J}_1^{\text{IMF}}(t) + 4m P_z \tau \left(X_2^{ik}(\theta_{\Delta_\perp}) - \frac{1}{2} \delta^{ik} \right) \mathcal{J}_2^{\text{IMF}}(t) \hat{Q}^{3k}, \\
\langle p', \lambda' | \hat{T}^{ij}(0) | p, \lambda \rangle &= 2m^2 \tau \left[\left(\frac{1}{3} \mathcal{D}_2^{\text{IMF}} - \frac{1}{2} \mathcal{D}_{(0,1)}^{\text{IMF}} \right) \delta_{\sigma'\sigma} + \left(-\frac{2}{3} \mathcal{D}_2^{\text{IMF}} - \frac{1}{2} \mathcal{D}_{(0,0)}^{\text{IMF}} \right) \delta_{\lambda'3} \delta_{\lambda 3} \right] \delta^{ij} \\
&\quad + 2m^2 \tau X_2^{ij}(\theta_{\Delta_\perp}) \left[\delta_{\sigma'\sigma} \mathcal{D}_{(0,1)}^{\text{IMF}}(t) + \delta_{\lambda'3} \delta_{\lambda 3} \mathcal{D}_{(0,0)}^{\text{IMF}}(t) \right] \\
&\quad + 4m^2 \tau \left[\hat{Q}^{ik} X_2^{jk}(\theta_{\Delta_\perp}) + \hat{Q}^{jk} X_2^{ik}(\theta_{\Delta_\perp}) - \hat{Q}^{lm} X_2^{lm}(\theta_{\Delta_\perp}) \delta^{ij} \right] \mathcal{D}_2^{\text{IMF}}(t) \\
&\quad + 8m^2 \tau^{3/2} i \epsilon^{lm3} \hat{S}^l X_1^m(\theta_{\Delta_\perp}) \left(X_2^{ij}(\theta_{\Delta_\perp}) - \frac{1}{2} \delta^{ij} \right) \mathcal{D}_1^{\text{IMF}}(t) \\
&\quad + 8m^2 \tau^2 \hat{Q}^{lm} \left(X_2^{lm}(\theta_{\Delta_\perp}) + \frac{1}{2} \delta^{lm} \right) \left(X_2^{ij}(\theta_{\Delta_\perp}) - \frac{1}{2} \delta^{ij} \right) \mathcal{D}_3^{\text{IMF}}(t),
\end{aligned} \tag{16}$$

where the multipole form factors are related to the GFFs in Eq. (11)

$$\begin{aligned}
\mathcal{E}_{(0,0)}^{\text{IMF}}(t) &= \frac{1}{3(1+\tau)^2} [12\tau\mathcal{J}_1 - 3(\tau-1)\mathcal{E}_0 + \tau(2+4\tau)\mathcal{E}_2 + \tau(\tau-1)(3\mathcal{D}_0 - 2\mathcal{D}_2) - 4\tau^2(1+2\tau)\mathcal{D}_3], \\
\mathcal{E}_{(0,1)}^{\text{IMF}}(t) &= \frac{1}{3(1+\tau)^2} [6\tau\mathcal{J}_1 + 3\mathcal{E}_0 - \tau\mathcal{E}_2 - 3\tau\mathcal{D}_0 - \tau\mathcal{D}_2 - 3\tau^2\mathcal{D}_2 + 2\tau^2\mathcal{D}_3], \\
\mathcal{E}_1^{\text{IMF}}(t) &= \frac{1}{3(1+\tau)^2} [-6(\tau-1)\mathcal{J}_1 - 6\mathcal{E}_0 + 2\tau\mathcal{E}_2 + 6\tau\mathcal{D}_0 - 4\tau(\mathcal{D}_2 + \tau\mathcal{D}_3)], \\
\mathcal{E}_2^{\text{IMF}}(t) &= -\frac{1}{3(1+\tau)^2} [6\mathcal{J}_1 - 3\mathcal{E}_0 - (3+2\tau)\mathcal{E}_2 + 3\tau\mathcal{D}_0 + (\tau+3)\mathcal{D}_2 + 2\tau(3+2\tau)\mathcal{D}_3], \\
\mathcal{J}_1^{\text{IMF}}(t) &= \frac{\mathcal{J}_1 - \tau\mathcal{D}_2}{1+\tau}, \quad \mathcal{J}_2^{\text{IMF}}(t) = \frac{\mathcal{J}_1 + \mathcal{D}_2}{1+\tau}, \\
\mathcal{D}_{(0,1)}^{\text{IMF}}(t) &= \mathcal{D}_0 + \frac{\tau}{3}G_W, \quad \mathcal{D}_{(0,0)}^{\text{IMF}}(t) = \mathcal{D}_0 + \frac{4\tau}{3}G_W, \\
\mathcal{D}_1^{\text{IMF}}(t) &= \frac{1}{4}G_W, \quad \mathcal{D}_2^{\text{IMF}}(t) = \mathcal{D}_2, \quad \mathcal{D}_3^{\text{IMF}}(t) = \mathcal{D}_3 - \frac{1}{4}G_W,
\end{aligned} \tag{17}$$

with

$$G_W(t) = -\frac{2(3\mathcal{D}_0 + \mathcal{D}_2 - 2\tau\mathcal{D}_3)}{3(1+\tau)}. \tag{18}$$

It is straightforward to understand the meaning of each term in Eq. (17). In the case of the 00 and 0*k*-components, they are subjected to both the Wigner spin rotation and get mixed with the other components of the EMT current under the Lorentz boost, so that they vary as shown in Eq. (17). It is remarkable to see that the dipole and quadrupole contributions are respectively induced by the Lorentz boost as shown in Eq. (16). When it comes to the matrix element of \hat{T}^{ij} , the *D*-term form factors undergo changes by the Wigner spin rotation under the Lorentz boost except for $\mathcal{D}_2^{\text{IMF}}(t)$. Interestingly, it was found that this effect of the Wigner spin rotation can be parametrized in terms of one combination of the form factors, G_W , as done for the EM form factors in Ref. [13]. In addition to that, the monopole form factors acquire the geometrical contribution in the presence of the quadrupole form factors. As shown in Eq. (14) there was no term such as $\mathcal{D}_1^{\text{IMF}}$ in the *ij*-component of the EMT current in the BF. It implies that the form factor $G_W(t)$ only appears by the Wigner spin rotation under the Lorentz boost. Thus, the induced dipole form factor $\mathcal{D}_1^{\text{IMF}}$ is solely due to the relativistic effect.

The multipole form factors at $t = 0$ in the IMF can be given as follows:

$$\begin{aligned}
\mathcal{E}_{(0,1)}^{\text{IMF}}(0) &= \mathcal{E}_{(0,0)}^{\text{IMF}}(0) = \mathcal{E}_0(0), \quad \mathcal{E}_1^{\text{IMF}}(0) = 2\mathcal{J}_1(0) - 2\mathcal{E}_0(0), \quad \mathcal{E}_2^{\text{IMF}}(0) = -2\mathcal{J}_1(0) + \mathcal{E}_0(0) + \mathcal{E}_2(0) - \mathcal{D}_2(0), \\
\mathcal{J}_1^{\text{IMF}}(0) &= \mathcal{J}_1(0), \quad \mathcal{J}_2^{\text{IMF}}(0) = \mathcal{J}_1(0) + \mathcal{D}_2(0), \\
\mathcal{D}_{(0,1)}^{\text{IMF}}(0) &= \mathcal{D}_{(0,0)}^{\text{IMF}}(0) = \mathcal{D}_0(0), \quad \mathcal{D}_1^{\text{IMF}}(0) = -\frac{1}{2}\mathcal{D}_0(0) - \frac{1}{6}\mathcal{D}_2(0), \\
\mathcal{D}_2^{\text{IMF}}(0) &= \mathcal{D}_2(0), \quad \mathcal{D}_3^{\text{IMF}}(0) = \mathcal{D}_3(0) + \left[\frac{1}{2}\mathcal{D}_0(0) + \frac{1}{6}\mathcal{D}_2(0) \right].
\end{aligned} \tag{19}$$

The results from the light-front formalism should coincide with those from the IMF. As a cross-check, we have carried out the same calculation in the light-front formalism (See Appendix A).

III. DEFINITION OF THE EMT DISTRIBUTIONS

While the 3D EMT distributions of a spin-one particle can not be interpreted as a probability densities because of the ambiguous relativistic corrections, we can understand it as a quasi-probabilistic distribution by the Wigner distribution. This quasi-probabilistic distribution conveys information on the internal structure of a hadron in a fully relativistic picture. The matrix element of the EMT current for a physical state $|\psi\rangle$ can be expressed in terms of the Wigner distribution as [25]

$$\langle \hat{T}^{\mu\nu}(\mathbf{r}) \rangle = \int \frac{d^3\mathbf{P}}{(2\pi)^3} \int d^3\mathbf{R} W(\mathbf{R}, \mathbf{P}) \langle \hat{T}^{\mu\nu}(\mathbf{r}) \rangle_{\mathbf{R}, \mathbf{P}}, \tag{20}$$

where $W(\mathbf{R}, \mathbf{P})$ represents the Wigner distribution given by

$$\begin{aligned} W(\mathbf{R}, \mathbf{P}) &= \int \frac{d^3 \Delta}{(2\pi)^3} e^{-i\Delta \cdot \mathbf{R}} \tilde{\psi}^* \left(\mathbf{P} + \frac{\Delta}{2} \right) \tilde{\psi} \left(\mathbf{P} - \frac{\Delta}{2} \right) \\ &= \int d^3 z e^{-iz \cdot \mathbf{P}} \psi^* \left(\mathbf{R} - \frac{\mathbf{z}}{2} \right) \psi \left(\mathbf{R} + \frac{\mathbf{z}}{2} \right). \end{aligned} \quad (21)$$

The average position \mathbf{R} and momentum \mathbf{P} are defined as $\mathbf{R} = (\mathbf{r}' + \mathbf{r})/2$ and $\mathbf{P} = (\mathbf{p}' + \mathbf{p})/2$, respectively. $\Delta = \mathbf{p}' - \mathbf{p}$ denotes the momentum transfer, which enables us to get access to the internal structure of a particle. The variable $\mathbf{z} = \mathbf{r}' - \mathbf{r}$ stands for the position separation between the initial and final particles. The Wigner distribution contains information on the wave packet of a particle

$$\psi(\mathbf{r}) = \langle \mathbf{r} | \psi \rangle = \int \frac{d^3 \mathbf{p}}{(2\pi)^3} e^{i\mathbf{p} \cdot \mathbf{r}} \tilde{\psi}(\mathbf{p}), \quad \tilde{\psi}(\mathbf{p}) = \frac{1}{\sqrt{2p^0}} \langle p | \psi \rangle, \quad (22)$$

with the plane-wave states $|p\rangle$ and $|\mathbf{r}\rangle$ respectively normalized as $\langle p' | p \rangle = 2p^0 (2\pi)^3 \delta^{(3)}(\mathbf{p}' - \mathbf{p})$ and $\langle \mathbf{r}' | \mathbf{r} \rangle = \delta^{(3)}(\mathbf{r}' - \mathbf{r})$. The position state $|\mathbf{r}\rangle$ localized at \mathbf{r} at time $t = 0$ is defined as a Fourier transform of the momentum eigenstate $|p\rangle$

$$|\mathbf{r}\rangle = \int \frac{d^3 \mathbf{p}}{(2\pi)^3 \sqrt{2p^0}} e^{-i\mathbf{p} \cdot \mathbf{r}} |p\rangle. \quad (23)$$

If we integrate over the average position and momentum, then the probabilistic density in either position or momentum space is recovered to be

$$\int \frac{d^3 \mathbf{P}}{(2\pi)^3} W_N(\mathbf{R}, \mathbf{P}) = |\psi_N(\mathbf{R})|^2, \quad \int d^3 \mathbf{R} W_N(\mathbf{R}, \mathbf{P}) = |\tilde{\psi}_N(\mathbf{P})|^2. \quad (24)$$

Given \mathbf{P} and \mathbf{R} , the matrix element $\langle \hat{T}^{\mu\nu}(\mathbf{r}) \rangle_{\mathbf{R}, \mathbf{P}}$ conveys information on the internal structure of the particle localized around the average position \mathbf{R} and average momentum \mathbf{P} . This can be expressed as the 3D Fourier transform of the matrix element $\langle p', \lambda' | \hat{T}^{\mu\nu}(0) | p, \lambda \rangle$:

$$\langle \hat{T}^{\mu\nu}(\mathbf{r}) \rangle_{\mathbf{R}, \mathbf{P}} = \langle \hat{T}^{\mu\nu}(0) \rangle_{-\mathbf{x}, \mathbf{0}} = \int \frac{d^3 \Delta}{(2\pi)^3} e^{-i\mathbf{x} \cdot \Delta} \frac{1}{\sqrt{2p^0} \sqrt{2p'^0}} \langle p', \lambda' | \hat{T}^{\mu\nu}(0) | p, \lambda \rangle, \quad (25)$$

with the shifted position vector $\mathbf{x} = \mathbf{r} - \mathbf{R}$. The matrix element $\langle p', \lambda' | \hat{T}^{\mu\nu}(0) | p, \lambda \rangle$ was discussed in the previous Section.

A. EMT distributions in the 3D Breit frame

Having integrated over \mathbf{P} of Eq. (20), we find that the part of the wave packet can be factorized. Thus, the target in the BF is understood as a localized state around \mathbf{R} from the Wigner perspective. In this frame, Eq. (25) is reduced to

$$T_{\text{BF}}^{\mu\nu}(\mathbf{x}, \lambda', \lambda) = \langle \hat{T}^{\mu\nu}(0) \rangle_{-\mathbf{x}, \mathbf{0}} = \int \frac{d^3 \Delta}{2P_0 (2\pi)^3} e^{-i\mathbf{x} \cdot \Delta} \langle p', \lambda' | \hat{T}^{\mu\nu}(0) | p, \lambda \rangle. \quad (26)$$

From now on we use \mathbf{r} instead of \mathbf{x} , i.e., $\mathbf{x} = \mathbf{r} - \mathbf{R} \rightarrow \mathbf{r}$. We expand the temporal component of the EMT distributions in terms of the multipole distributions as follows:

$$T_{\text{BF}}^{00}(\mathbf{r}, \lambda', \lambda) = \varepsilon_0(r) \delta_{\lambda' \lambda} + \varepsilon_2(r) \hat{Q}^{ij} Y_2^{ij}(\Omega_r), \quad (27)$$

where

$$\varepsilon_0(r) = m \tilde{\mathcal{E}}_0(r), \quad \varepsilon_2(r) = -\frac{1}{2m} r \frac{d}{dr} \frac{1}{r} \frac{d}{dr} \tilde{\mathcal{E}}_2(r), \quad (28)$$

with

$$\tilde{\mathcal{E}}_{0,2}(r) = 2m \int \frac{d^3 \Delta}{2P_0 (2\pi)^3} e^{-i\Delta \cdot \mathbf{r}} \mathcal{E}_{0,2}(t). \quad (29)$$

Note that since the angle integration of Y_2^{ij} vanishes, i.e., $\int d\Omega_r Y_2^{ij}(\Omega_r) = 0$, we have the normalization of the mass distribution $\mathcal{E}_0(0)$ as follows:

$$\int d^3r T_{\text{BF}}^{00}(\mathbf{r}, \lambda', \lambda) = \int d^3r \varepsilon_0(r) \delta_{\lambda'\lambda} = m\mathcal{E}_0(0) \delta_{\lambda'\lambda}, \quad (30)$$

which gives $\mathcal{E}_0(0) = 1$.

We can get the spin distribution by contracting T_{BF}^{0k} by $\epsilon^{ijk} r^j$

$$\begin{aligned} J^i(\mathbf{r}, \lambda', \lambda) &= \epsilon^{ijk} r^j T_{\text{BF}}^{0k}(\mathbf{r}, \lambda', \lambda) \\ &= \hat{S}_{\lambda'\lambda}^j \int \frac{d^3\Delta}{(2\pi)^3} e^{-i\mathbf{r}\cdot\Delta} \left[\left(\bar{\mathcal{J}}_1(t) + \frac{2}{3}t \frac{d\bar{\mathcal{J}}_1(t)}{dt} \right) \delta^{ij} + \left(\Delta^i \Delta^j - \frac{1}{3}\Delta^2 \delta^{ij} \right) \frac{d\bar{\mathcal{J}}_1(t)}{dt} \right] \end{aligned} \quad (31)$$

with $\bar{\mathcal{J}}_1 := m\mathcal{J}_1/P_0$. Integrating the angular-momentum distribution J^i over \mathbf{r} yields $\int d^3r J^i(\mathbf{r}, \lambda', \lambda) = \hat{S}_{\lambda'\lambda}^i \mathcal{J}_1(0)$, so that we have the obvious normalization for spin, i.e., $\mathcal{J}_1(0) = 1$.

The spatial component of the EMT distributions can be parametrized in terms of the elastic pressure and shear forces, given by[41]

$$\begin{aligned} T_{\text{BF}}^{ij}(\mathbf{r}, \lambda', \lambda) &= p_0(r) \delta^{ij} + s_0(r) Y_2^{ij}(\Omega_r) + p_2(r) \hat{Q}^{ij} + s_2(r) 2 \left[\hat{Q}^{ip} Y_2^{pj}(\Omega_r) + \hat{Q}^{jp} Y_2^{pi}(\Omega_r) - \delta^{ij} \hat{Q}^{pq} Y_2^{pq}(\Omega_r) \right] \\ &\quad - \frac{1}{m^2} \hat{Q}^{pq} \partial^p \partial^q \left[p_3(r) \delta^{ij} + s_3(r) Y_2^{ij}(\Omega_r) \right], \end{aligned} \quad (32)$$

where

$$p_n(r) = \frac{1}{6m} \frac{1}{r^2} \frac{d}{dr} r^2 \frac{d}{dr} \tilde{\mathcal{D}}_n(r), \quad s_n(r) = -\frac{1}{4m} r \frac{d}{dr} \frac{1}{r} \frac{d}{dr} \tilde{\mathcal{D}}_n(r) \quad (33)$$

with

$$\tilde{\mathcal{D}}_n(r) = 2m \int \frac{d^3\Delta}{2P_0(2\pi)^3} e^{-i\Delta\cdot\mathbf{r}} \mathcal{D}_n(t). \quad (34)$$

The conservation of the EMT current furnishes the equilibrium conditions as

$$p'_n(r) + \frac{2}{3}s'_n(r) + \frac{2}{r}s_n(r) = 0, \quad (n = 0, 2, 3). \quad (35)$$

The pressures given in Eq. (33) satisfy the von Laue conditions:

$$\int d^3r p_n(r) = 0. \quad (36)$$

Note that all the monopole and quadrupole distributions are related to the dimensionless constant D -terms

$$\mathcal{D}_n(0) = m \int d^3r r^2 p_n(r) = -\frac{4}{15} m \int d^3r r^2 s_n(r), \quad (n = 0, 2, 3). \quad (37)$$

B. EMT distributions in the 2D Breit frame

The EF distributions depend on the impact parameter x_\perp ($\mathbf{r} = (\mathbf{x}_\perp, x_z)$) and momentum $\mathbf{P} = (\mathbf{0}, P_z)$ where a spin-one particle moves along the z -direction without loss of generality. In this frame, Eq. (25) is reduced to

$$T_{\text{EF}}^{\mu\nu}(\mathbf{x}_\perp, P_z, \lambda', \lambda) := \int dx_z \langle \hat{T}^{\mu\nu}(0) \rangle_{-\mathbf{r}, \mathbf{0}} = \int \frac{d^2\Delta_\perp}{2P_0(2\pi)^2} e^{-i\mathbf{x}_\perp \cdot \Delta_\perp} \langle p', \lambda' | \hat{T}^{\mu\nu}(0) | p, \lambda \rangle \Big|_{\Delta_z=0}. \quad (38)$$

Before investigating the EMT distributions in the IMF, one should first separate the geometrical contributions from the relativistic ones. By doing that, we can explicitly show that the relativistic corrections are different from the geometrical ones.

In this subsection, we examine the distributions in the 2D BF by taking $P_z \rightarrow 0$. The temporal component of the EMT current in the 2D EF is given by

$$T_{\text{EF}}^{00}(\mathbf{x}_\perp, 0, \lambda', \lambda) = \delta_{3\lambda} \delta_{\lambda'3} \varepsilon_{(0,0)}^{(2\text{D})}(\mathbf{x}_\perp) + \delta_{\sigma'\sigma} \varepsilon_{(0,1)}^{(2\text{D})}(\mathbf{x}_\perp) + \hat{Q}^{ij} X_2^{ij}(\theta_{\mathbf{x}_\perp}) \varepsilon_2^{(2\text{D})}(\mathbf{x}_\perp). \quad (39)$$

The mass distribution is defined by

$$\varepsilon_{(0,l)}^{(2\text{D})}(\mathbf{x}_\perp) = m \tilde{\mathcal{E}}_{(0,l)}(\mathbf{x}_\perp), \quad \varepsilon_2^{(2\text{D})}(\mathbf{x}_\perp) = -\frac{1}{2m} x_\perp \frac{d}{dx_\perp} \frac{1}{x_\perp} \frac{d}{dx_\perp} \tilde{\mathcal{E}}_2(\mathbf{x}_\perp), \quad (40)$$

where

$$\tilde{\mathcal{E}}_{(0,l),2}(\mathbf{x}_\perp) = 2m \int \frac{d^2 \Delta}{2P_0(2\pi)^2} e^{-i\Delta_\perp \cdot \mathbf{x}_\perp} \mathcal{E}_{(0,l),2}(t), \quad (l = 0, 1). \quad (41)$$

At the zero momentum transfer $t = 0$, the normalizations of the form factors in the 2D BF are found to be

$$\mathcal{E}_{(0,l)}(0) = \frac{1}{m} \int d^2 x_\perp \varepsilon_{(0,l)}^{(2\text{D})}(\mathbf{x}_\perp), \quad \mathcal{E}_2(0) = -\frac{m}{4} \int d^2 x_\perp x_\perp^2 \varepsilon_2^{(2\text{D})}(\mathbf{x}_\perp), \quad \text{with } (l = 0, 1). \quad (42)$$

One can see that the newly introduced form factors $\mathcal{E}_{(0,l)}$ are normalized to be $\mathcal{E}_{(0,0)}(0) = \mathcal{E}_{(0,1)}(0) = \mathcal{E}(0) = 1$ from Eq. (15). These features will be revisited in Secion IV.

We obtain the spin distribution as

$$J_{(2\text{D})}^3(\mathbf{x}_\perp, \lambda', \lambda) = \epsilon^{3jk} x_\perp^j T_{\text{EF}}^{0k}(\mathbf{x}_\perp, 0, \lambda', \lambda) = \hat{S}_{\lambda'\lambda}^3 \int \frac{d^2 \Delta}{(2\pi)^2} e^{-i\mathbf{x}_\perp \cdot \Delta_\perp} \left[\bar{\mathcal{J}}_1(t) + t \frac{d\bar{\mathcal{J}}_1(t)}{dt} \right] \quad (43)$$

with $\bar{\mathcal{J}}_1(t) := m\mathcal{J}_1(t)/P_0$. Integrating the 2D angular-momentum distribution $J_{(2\text{D})}^3$ over \mathbf{x}_\perp yields $\int d^2 x_\perp J_{(2\text{D})}^3(\mathbf{x}_\perp, \lambda', \lambda) = \hat{S}_{\lambda'\lambda}^3 \mathcal{J}_1(0)$, so that we get the normalization for spin, i.e., $\mathcal{J}_1(0) = 1$. It gives exactly the same constraint given in Eq. (31).

As done in the 3D case, the spatial component of the EMT distributions in the EF can be constructed as follows

$$\begin{aligned} T_{\text{EF}}^{ij}(\mathbf{x}_\perp, 0, \lambda', \lambda) &= \int \frac{d^2 \Delta}{2P_0(2\pi)^2} e^{-i\Delta_\perp \cdot \mathbf{x}_\perp} \langle p', \lambda' | \hat{T}^{ij}(0) | p, \lambda \rangle \\ &= \left(p_0^{(2\text{D})}(\mathbf{x}_\perp) - \frac{2}{3} p_2^{(2\text{D})}(\mathbf{x}_\perp) \right) \delta^{ij} \delta_{\sigma'\sigma} + s_0^{(2\text{D})}(\mathbf{x}_\perp) X_2^{ij}(\theta_{\mathbf{x}_\perp}) \delta_{\sigma'\sigma} \\ &+ \left(p_0^{(2\text{D})}(\mathbf{x}_\perp) + \frac{4}{3} p_2^{(2\text{D})}(\mathbf{x}_\perp) \right) \delta^{ij} \delta_{\lambda'3} \delta_{\lambda 3} + s_0^{(2\text{D})}(\mathbf{x}_\perp) X_2^{ij}(\theta_{\mathbf{x}_\perp}) \delta_{\lambda'3} \delta_{\lambda 3} \\ &+ 2s_2^{(2\text{D})}(\mathbf{x}_\perp) \left[\hat{Q}^{ip} X_2^{pj}(\theta_{\mathbf{x}_\perp}) + \hat{Q}^{jp} X_2^{pi}(\theta_{\mathbf{x}_\perp}) - \delta^{ij} \hat{Q}^{pq} X_2^{pq}(\theta_{\mathbf{x}_\perp}) \right] \\ &- \frac{1}{m^2} \hat{Q}^{pq} \partial^p \partial^q \left(s_3^{(2\text{D})}(\mathbf{x}_\perp) X^{ij}(\theta_{\mathbf{x}_\perp}) + p_3^{(2\text{D})}(\mathbf{x}_\perp) \delta^{ij} \right), \end{aligned} \quad (44)$$

where $p_n^{(2\text{D})}(\mathbf{x}_\perp)$ and $s_n^{(2\text{D})}(\mathbf{x}_\perp)$ are expressed as

$$p_n^{(2\text{D})}(\mathbf{x}_\perp) = \frac{1}{8m} \frac{1}{x_\perp} \frac{d}{dx_\perp} x_\perp \frac{d}{dx_\perp} \tilde{\mathcal{D}}_n(\mathbf{x}_\perp), \quad s_n^{(2\text{D})}(\mathbf{x}_\perp) = -\frac{1}{4m} x_\perp \frac{d}{dx_\perp} \frac{1}{x_\perp} \frac{d}{dx_\perp} \tilde{\mathcal{D}}_n(\mathbf{x}_\perp) \quad (45)$$

with

$$\tilde{\mathcal{D}}_n(\mathbf{x}_\perp) = 2m \int \frac{d^2 \Delta}{2E(2\pi)^2} e^{-i\Delta_\perp \cdot \mathbf{x}_\perp} \mathcal{D}_n(t). \quad (46)$$

A remarkable difference between 2D BF and 3D BF distributions is that the $p_2^{(2\text{D})}$ distribution is induced to the monopole structure as shown in the mass distribution, which should be distinguished from the relativistic effects that will be discussed later. One can find the monopole term of T_{EF}^{ij} in Eq. (44). As previously shown, we obtain the equilibrium conditions by the conservation of the EMT current

$$p_n^{(2\text{D})\prime}(\mathbf{x}_\perp) + \frac{1}{2} s_n^{(2\text{D})\prime}(\mathbf{x}_\perp) + \frac{1}{r} s_n^{(2\text{D})}(\mathbf{x}_\perp) = 0, \quad (n = 0, 2, 3), \quad (47)$$

which result in the von Laue stability conditions for all the monopole and quadrupole pressures:

$$\int d^2x_{\perp} p_n^{(2D)}(x_{\perp}) = 0. \quad (48)$$

They are related to the dimensionless constant D -terms

$$\mathcal{D}_n(0) = 2m \int d^2x_{\perp} x_{\perp}^2 p_n^{(2D)}(x_{\perp}) = -\frac{1}{2}m \int d^2x_{\perp} x_{\perp}^2 s_n^{(2D)}(x_{\perp}), \quad (n = 0, 2, 3). \quad (49)$$

Once we have the spatial component of the EMT distributions, we can look into how the 2D stress tensor provides information on the internal forces that make a hadron stable. It would be interesting to investigate the strong force fields and visualize them in 2D space. The internal local force fields are given by

$$\hat{\mathbf{x}}_{\perp}^i T_{\text{EF}}^{ij}(\mathbf{x}_{\perp}, 0, \lambda', \lambda) = \frac{dF_r}{dS_r} \hat{\mathbf{x}}_{\perp}^j + \frac{dF_{\theta}}{dS_{\theta}} \hat{\boldsymbol{\theta}}_{\perp}^j, \quad \hat{\boldsymbol{\theta}}_{\perp}^i T_{\text{EF}}^{ij}(\mathbf{x}_{\perp}, 0, \lambda', \lambda) = \frac{dF_r}{dS_{\theta}} \hat{\mathbf{x}}_{\perp}^j + \frac{dF_{\theta}}{dS_{\theta}} \hat{\boldsymbol{\theta}}_{\perp}^j. \quad (50)$$

Each force field acting on the infinitesimal area is derived as

$$\begin{aligned} \frac{dF_r}{dS_r} &= \left[\left(p_0^{(2D)} + \frac{1}{2} s_0^{(2D)} \right) - \frac{1}{3} \left(2p_2^{(2D)} + s_2^{(2D)} + \frac{1}{m^2} \left[-\frac{s_3^{(2D)'}}{2x_{\perp}} - \frac{p_3^{(2D)'}}{x_{\perp}} + \frac{2s_3^{(2D)}}{x_{\perp}^2} \right] \right) \right] \delta_{\sigma'\sigma} \\ &+ \left[\left(p_0^{(2D)} + \frac{1}{2} s_0^{(2D)} \right) + \frac{2}{3} \left(2p_2^{(2D)} + s_2^{(2D)} + \frac{1}{m^2} \left[-\frac{s_3^{(2D)'}}{2x_{\perp}} - \frac{p_3^{(2D)'}}{x_{\perp}} + \frac{2s_3^{(2D)}}{x_{\perp}^2} \right] \right) \right] \delta_{\lambda'3} \delta_{3\lambda} \\ &+ \hat{Q}_{\lambda'\lambda}^{rr} \frac{1}{m^2} \left[-p_3^{(2D)''} + \frac{p_3^{(2D)'}}{x_{\perp}} - \frac{s_3^{(2D)''}}{2} + \frac{s_3^{(2D)'}}{2x_{\perp}} - \frac{2s_3^{(2D)}}{x_{\perp}^2} \right], \\ \frac{dF_{\theta}}{dS_{\theta}} &= \frac{dF_r}{dS_r} = \hat{Q}_{\lambda'\lambda}^{r\theta} \frac{1}{m^2} \left[-\frac{2s_3^{(2D)'}}{x_{\perp}} + \frac{2s_3^{(2D)}}{x_{\perp}^2} \right], \\ \frac{dF_{\theta}}{dS_{\theta}} &= \left[\left(p_0^{(2D)} - \frac{1}{2} s_0^{(2D)} \right) - \frac{1}{3} \left(2p_2^{(2D)} + s_2^{(2D)} + \frac{1}{m^2} \left[\frac{s_3^{(2D)'}}{2x_{\perp}} - \frac{p_3^{(2D)'}}{x_{\perp}} \right] \right) \right] \delta_{\sigma'\sigma} \\ &+ \left[\left(p_0^{(2D)} - \frac{1}{2} s_0^{(2D)} \right) + \frac{2}{3} \left(2p_2^{(2D)} + s_2^{(2D)} + \frac{1}{m^2} \left[\frac{s_3^{(2D)'}}{2x_{\perp}} - \frac{p_3^{(2D)'}}{x_{\perp}} \right] \right) \right] \delta_{\lambda'3} \delta_{3\lambda} \\ &+ \hat{Q}_{\lambda'\lambda}^{rr} \left(-2s_2^{(2D)} + \frac{1}{m^2} \left[-p_3^{(2D)''} + \frac{p_3^{(2D)'}}{x_{\perp}} + \frac{s_3^{(2D)''}}{2} - \frac{s_3^{(2D)'}}{2x_{\perp}} \right] \right) + \hat{Q}_{\lambda'\lambda}^{\theta\theta} \left[-2s_2^{(2D)} - \frac{2}{m^2} \frac{s_3^{(2D)}}{x_{\perp}^2} \right]. \quad (51) \end{aligned}$$

If the target is polarized along the longitudinal direction, there is no θ dependence in the infinitesimal forces, such as $\hat{Q}_{33}^{rr} = \hat{Q}_{33}^{\theta\theta} = 1/3$ and $\hat{Q}_{33}^{r\theta} = 0$. However, if a target is polarized along one axis of the transverse plane, the angle dependence on θ appears (see Appendix C).

C. EMT densities in the 2D infinite momentum frame

As mentioned previously, the EMT densities in the 2D IMF do not require any relativistic corrections, so that they have a probabilistic meaning. In the IMF, we divide the mass and mechanical densities respectively by the Lorentz factors P_0/m and m/P_0 to remove the kinematical divergence and suppression in these densities:

$$\begin{aligned} T_{\text{IMF}}^{00}(\mathbf{x}_{\perp}, \lambda', \lambda) &:= T_{\text{EF}}^{00}(\mathbf{x}_{\perp}, P_z, \lambda', \lambda) \frac{m}{P_0} \Big|_{P_z \rightarrow \infty}, \\ T_{\text{IMF}}^{ij}(\mathbf{x}_{\perp}, \lambda', \lambda) &:= T_{\text{EF}}^{ij}(\mathbf{x}_{\perp}, P_z, \lambda', \lambda) \frac{P_0}{m} \Big|_{P_z \rightarrow \infty}. \quad (52) \end{aligned}$$

Thus, the T_{IMF}^{00} is normalized to be its mass m instead of its momentum P_z . This normalization is the same as the T_{BF}^{00} one. One should keep in mind that this mass density $\sim mT^{++}/P^+$ is actually connected to the momentum density T^{++} defined in the light-cone basis. It is different from the higher-twist mass density that arises from the

bad component of the EMT current. In this paper, the *mass density in 2D IMF* indicates the momentum density normalized as a hadron mass. Similarly, the normalization of the T_{IMF}^{ij} is consistent with that of T_{BF}^{ij} . The temporal component of the EMT current in the 2D IMF is given by

$$T_{\text{IMF}}^{00}(\mathbf{x}_\perp, \lambda', \lambda) = \delta_{3\lambda}\delta_{\lambda'3}\varepsilon_{(0,0)}^{\text{IMF}}(x_\perp) + \delta_{\sigma'\sigma}\varepsilon_{(0,1)}^{\text{IMF}}(x_\perp) + \epsilon^{3jk}\hat{S}^j X_1^k(\theta_{x_\perp})\varepsilon_1^{\text{IMF}}(x_\perp) + \hat{Q}^{ij} X_2^{ij}(\theta_{x_\perp})\varepsilon_2^{\text{IMF}}(x_\perp), \quad (53)$$

where 2D mass densities in the IMF are defined as

$$\varepsilon_{(0,l)}^{\text{IMF}}(x_\perp) = m\tilde{\mathcal{E}}_{(0,l)}^{\text{IMF}}(x_\perp), \quad \varepsilon_1^{\text{IMF}}(x_\perp) = -\frac{1}{2}\frac{d}{dx_\perp}\tilde{\mathcal{E}}_1^{\text{IMF}}(x_\perp), \quad \varepsilon_2^{\text{IMF}}(x_\perp) = -\frac{1}{2m}x_\perp\frac{d}{dx_\perp}\frac{1}{x_\perp}\frac{d}{dx_\perp}\tilde{\mathcal{E}}_2^{\text{IMF}}(x_\perp) \quad (54)$$

with

$$\tilde{\mathcal{E}}_{(0,l),n}^{\text{IMF}}(x_\perp) = \int \frac{d^2\Delta}{(2\pi)^2} e^{-i\Delta\cdot r} \mathcal{E}_{(0,l),n}^{\text{IMF}}(t), \quad (n = 1, 2 \text{ and } l = 0, 1). \quad (55)$$

As discussed in the 2D BF, the geometrical difference between 2D and 3D space brings about the induced monopole term. It contributes to $\varepsilon_{(0,l)}^{\text{IMF}}$ together with the 3D BF distribution. In addition to that, $\varepsilon_{(0,l)}^{\text{IMF}}$ is subject to the relativistic effects arising from the Lorentz boost. On the other hand, the $\varepsilon_2^{\text{IMF}}$ consists of the pure 3D BF distribution together with the relativistic effects.

Interestingly, the dipole mass density is induced in the 2D IMF as shown in Eq. (53). On the other hand, the 2D BF mass distributions in Eq. (B1) do not contain the dipole one. It implies that the dipole mass density for a spin-1 particle is induced by the Lorentz boost. At the zero momentum transfer $t = 0$, the normalizations of the GFFs in the 2D IMF are found to be

$$\mathcal{E}_{(0,l)}^{\text{IMF}}(0) = \frac{1}{m} \int d^2x_\perp \varepsilon_{(0,l)}^{\text{IMF}}(x_\perp), \quad \mathcal{E}_2^{\text{IMF}}(0) = -\frac{m}{4} \int d^2x_\perp x_\perp^2 \varepsilon_2^{\text{IMF}}(x_\perp), \quad \text{with } (l = 1, 2). \quad (56)$$

Since the 2D angle integration of the irreducible tensor $X_n^{i\dots i_n}$, we obtain the normalization of the 2D mass distributions

$$\begin{aligned} \int d^2x_\perp T_{\text{IMF}}^{00}(\mathbf{x}_\perp, \lambda', \lambda) &= \int d^2x_\perp \left[\varepsilon_{(0,0)}^{\text{IMF}}(x_\perp)\delta_{\lambda'3}\delta_{3\lambda} + \varepsilon_{(0,1)}^{\text{IMF}}(x_\perp)\delta_{\sigma'\sigma} \right] \\ &= m \left[\mathcal{E}_{(0,0)}^{\text{IMF}}(0)\delta_{\lambda'3}\delta_{3\lambda} + \mathcal{E}_{(0,1)}^{\text{IMF}}(0)\delta_{\sigma'\sigma} \right]. \end{aligned} \quad (57)$$

As shown in Eq. (19), we find $\mathcal{E}_{(0,0)}^{\text{IMF}}(0) = \mathcal{E}_{(0,1)}^{\text{IMF}}(0) = \mathcal{E}_0(0) = 1$, so the T_{IMF}^{00} is properly normalized to its mass regardless of its spin polarization. We want to mention that the normalizations of the mass and spin lead to $\mathcal{E}_1^{\text{IMF}}(0) = 2\mathcal{J}_1(0) - 2\mathcal{E}_0(0) = 0$ in Eq. (19), which yields the interesting non-trivial constraint on the induced dipole mass density:

$$\mathcal{E}_1^{\text{IMF}}(0) = \int d^2x_\perp x_\perp \varepsilon_1^{\text{IMF}}(x_\perp) = 0. \quad (58)$$

The spin density is obtained as

$$\begin{aligned} J_{\text{IMF}}^3(\mathbf{x}_\perp, \lambda', \lambda) &= \epsilon^{3jk} x_\perp^j T_{\text{EF}}^{0k}(\mathbf{x}_\perp, P_z, \lambda', \lambda) \Big|_{P_z \rightarrow \infty} \\ &= \hat{S}_{\lambda'\lambda}^3 \int \frac{d^2\Delta}{(2\pi)^2} e^{-i\mathbf{x}_\perp \cdot \Delta_\perp} \left[\mathcal{J}_1(t) + t \frac{d\mathcal{J}_1(t)}{dt} \right] \\ &+ i\epsilon^{3jl} \hat{Q}_{\lambda'\lambda}^{3l} \frac{1}{2m} \int \frac{d^2\Delta}{(2\pi)^2} e^{-i\mathbf{x}_\perp \cdot \Delta_\perp} \Delta^j \left[3\mathcal{J}_2(t) + 2t \frac{d\mathcal{J}_2(t)}{dt} \right]. \end{aligned} \quad (59)$$

Note that in the IMF the induced quadrupole structure yields the additional contribution to the spin densities. The integration of J_{IMF}^3 over \mathbf{x}_\perp removes the quadrupole contribution, except for \mathcal{J}_1 . We thus have same normalization $\int d^2x_\perp J_{\text{IMF}}^3(\mathbf{x}_\perp, \lambda', \lambda) = \hat{S}_{\lambda'\lambda}^3 \mathcal{J}_1(0)$ with $\mathcal{J}_1(0) = 1$ as in the case of the 2D BF spin distribution.

We can derive the spatial component of the EMT densities in the 2D IMF as follows

$$\begin{aligned}
T_{\text{IMF}}^{ij}(\mathbf{x}_\perp, \lambda', \lambda) &= \left(p_{(0,1)}^{\text{IMF}}(x_\perp) - \frac{2}{3} p_2^{\text{IMF}}(x_\perp) \right) \delta_{\sigma'\sigma} \delta^{ij} + s_{(0,1)}^{\text{IMF}}(x_\perp) \delta_{\sigma'\sigma} X_2^{ij}(\theta_{x_\perp}) \\
&+ \left(p_{(0,0)}^{\text{IMF}}(x_\perp) + \frac{4}{3} p_2^{\text{IMF}}(x_\perp) \right) \delta_{\lambda'3} \delta_{\lambda 3} \delta^{ij} + s_{(0,0)}^{\text{IMF}}(x_\perp) \delta_{\lambda'3} \delta_{\lambda 3} X_2^{ij}(\theta_{x_\perp}) \\
&+ 2s_2^{\text{IMF}}(x_\perp) \left[\hat{Q}^{ip} X_2^{pj}(\theta_{x_\perp}) + \hat{Q}^{jp} X_2^{pi}(\theta_{x_\perp}) - \delta^{ij} \hat{Q}^{pq} X_2^{pq}(\theta_{x_\perp}) \right] \\
&- \frac{1}{m^2} \hat{Q}^{pq} \partial^p \partial^q \left(s_3^{\text{IMF}}(x_\perp) X_2^{ij}(\theta_{x_\perp}) + p_3^{\text{IMF}}(x_\perp) \delta^{ij} \right) \\
&- \frac{2}{m} \epsilon^{lm3} \hat{S}^l \partial^m \left(s_1^{\text{IMF}}(x_\perp) X_2^{ij}(\theta_{x_\perp}) + p_1^{\text{IMF}}(x_\perp) \delta^{ij} \right).
\end{aligned} \tag{60}$$

We then have five different equilibrium conditions:

$$p_{(0,l),n}^{\text{IMF}'}(x_\perp) + \frac{1}{2} s_{(0,l),n}^{\text{IMF}'}(x_\perp) + \frac{1}{x_\perp} s_{(0,l),n}^{\text{IMF}}(x_\perp) = 0, \quad (n = 1, 2, 3 \text{ and } l = 0, 1), \tag{61}$$

where $p_{(0,l),n}^{\text{IMF}}$ and $s_{(0,l),n}^{\text{IMF}}$ are defined as

$$p_{(0,l),n}^{\text{IMF}}(x_\perp) = \frac{1}{8m} \frac{1}{x_\perp} \frac{d}{dx_\perp} x_\perp \frac{d}{dx_\perp} \tilde{\mathcal{D}}_{(0,l),n}^{\text{IMF}}(x_\perp), \quad s_{(0,l),n}^{\text{IMF}}(x_\perp) = -\frac{1}{4m} x_\perp \frac{d}{dx_\perp} \frac{1}{x_\perp} \frac{d}{dx_\perp} \tilde{\mathcal{D}}_{(0,l),n}^{\text{IMF}}(x_\perp), \tag{62}$$

with

$$\tilde{\mathcal{D}}_{(0,l),n}^{\text{IMF}}(x_\perp) = \int \frac{d^2 \Delta}{(2\pi)^2} e^{-i\Delta_\perp \cdot \mathbf{x}_\perp} \mathcal{D}_{(0,l),n}^{\text{IMF}}(t), \quad (n = 1, 2, 3 \text{ and } l = 0, 1). \tag{63}$$

The difference between 2D BF and 2D IMF pressure and shear force distributions solely results from the Lorentz boost effects. In addition to that, p_1^{IMF} and s_1^{IMF} purely originate from the Lorentz boost effects. All the pressure densities satisfy the von Laue condition:

$$\int d^2 x_\perp p_{(0,l),n}^{\text{IMF}}(x_\perp) = 0. \tag{64}$$

They are related to the constant D -terms

$$\mathcal{D}_{(0,l),n}^{\text{IMF}}(0) = 2m \int d^2 x_\perp x_\perp^2 p_{(0,l),n}^{\text{IMF}}(x_\perp) = -\frac{1}{2} m \int d^2 x_\perp x_\perp^2 s_{(0,l),n}^{\text{IMF}}(x_\perp), \quad (n = 1, 2, 3 \text{ and } l = 0, 1) \tag{65}$$

The internal local force fields in the IMF are given by

$$\hat{\mathbf{x}}_\perp^i T_{\text{IMF}}^{ij}(\mathbf{x}_\perp, \lambda', \lambda) = \frac{dF_r}{dS_r} \hat{\mathbf{x}}_\perp^j + \frac{dF_\theta}{dS_r} \hat{\boldsymbol{\theta}}_\perp^j, \quad \hat{\boldsymbol{\theta}}_\perp^i T_{\text{IMF}}^{ij}(\mathbf{x}_\perp, \lambda', \lambda) = \frac{dF_r}{dS_\theta} \hat{\mathbf{x}}_\perp^j + \frac{dF_\theta}{dS_\theta} \hat{\boldsymbol{\theta}}_\perp^j, \tag{66}$$

where

$$\begin{aligned}
\frac{dF_r}{dS_r} &= \left[\left(p_{(0,1)}^{\text{IMF}} + \frac{1}{2} s_{(0,1)}^{\text{IMF}} \right) - \frac{1}{3} \left(2p_2^{\text{IMF}} + s_2^{\text{IMF}} + \frac{1}{m^2} \left[-\frac{s_3^{\text{IMF}'}}{2x_\perp} - \frac{p_3^{\text{IMF}'}}{x_\perp} + \frac{2s_3^{\text{IMF}}}{x_\perp^2} \right] \right) \right] \delta_{\sigma'\sigma} \\
&+ \left[\left(p_{(0,0)}^{\text{IMF}} + \frac{1}{2} s_{(0,0)}^{\text{IMF}} \right) + \frac{2}{3} \left(2p_2^{\text{IMF}} + s_2^{\text{IMF}} + \frac{1}{m^2} \left[-\frac{s_3^{\text{IMF}'}}{2x_\perp} - \frac{p_3^{\text{IMF}'}}{x_\perp} + \frac{2s_3^{\text{IMF}}}{x_\perp^2} \right] \right) \right] \delta_{\lambda'3} \delta_{3\lambda} \\
&+ \hat{Q}_{\lambda'\lambda}^{rr} \frac{1}{m^2} \left[-p_3^{\text{IMF}''} + \frac{p_3^{\text{IMF}'}}{x_\perp} - \frac{s_3^{\text{IMF}''}}{2} + \frac{s_3^{\text{IMF}'}}{2x_\perp} - \frac{2s_3^{\text{IMF}}}{x_\perp^2} \right] - \epsilon^{lm3} \hat{S}^l X_1^m(\theta_{x_\perp}) \frac{1}{m} [2p_1^{\text{IMF}'} + s_1^{\text{IMF}'}], \\
\frac{dF_r}{dS_\theta} &= \frac{dF_\theta}{dS_r} = \hat{Q}_{\lambda'\lambda}^{r\theta} \frac{1}{m^2} \left[-\frac{2s_3^{\text{IMF}'}}{x_\perp} + \frac{2s_3^{\text{IMF}}}{x_\perp^2} \right] - \frac{2}{m} \epsilon^{lm3} \hat{S}^l \hat{\theta}_\perp^m \frac{s_1^{\text{IMF}}}{x_\perp}, \\
\frac{dF_\theta}{dS_\theta} &= \left[\left(p_{(0,1)}^{\text{IMF}} - \frac{1}{2} s_{(0,1)}^{\text{IMF}} \right) - \frac{1}{3} \left(2p_2^{\text{IMF}} + s_2^{\text{IMF}} + \frac{1}{m^2} \left[\frac{s_3^{\text{IMF}'}}{2x_\perp} - \frac{p_3^{\text{IMF}'}}{x_\perp} \right] \right) \right] \delta_{\sigma'\sigma} \\
&+ \left[\left(p_{(0,0)}^{\text{IMF}} - \frac{1}{2} s_{(0,0)}^{\text{IMF}} \right) + \frac{2}{3} \left(2p_2^{\text{IMF}} + s_2^{\text{IMF}} + \frac{1}{m^2} \left[\frac{s_3^{\text{IMF}'}}{2x_\perp} - \frac{p_3^{\text{IMF}'}}{x_\perp} \right] \right) \right] \delta_{\lambda'3} \delta_{3\lambda} \\
&+ \hat{Q}_{\lambda'\lambda}^{rr} \left(-2s_2^{\text{IMF}} + \frac{1}{m^2} \left[-p_3^{\text{IMF}''} + \frac{p_3^{\text{IMF}'}}{x_\perp} + \frac{s_3^{\text{IMF}''}}{2} - \frac{s_3^{\text{IMF}'}}{2x_\perp} \right] \right) + \hat{Q}_{\lambda'\lambda}^{\theta\theta} \left[-2s_2^{\text{IMF}} - \frac{2}{m^2} \frac{s_3^{\text{IMF}}}{x_\perp^2} \right] \\
&- \epsilon^{lm3} \hat{S}^l X_1^m(\theta_{x_\perp}) \frac{1}{m} [2p_1^{\text{IMF}'} - s_1^{\text{IMF}'}]. \tag{67}
\end{aligned}$$

IV. ABEL TRANSFORMATION FOR THE SPIN-1 PARTICLE

In the case of the nucleon EM form factors [28], the 3D BF charge distributions are distinguished from 2D IMF charge densities by the relativistic factor $\sqrt{1-t/4m^2}$ in the integrand of the Fourier transform of the EM form factors. Since the relativistic factor generates the infinite order of the Laplacians, it is technically difficult to connect the 3D charge distributions in the BF to the 2D charge densities in IMF. It requires us to impose the infinite number of boundary conditions on the differential equation. As for the Abel transformation for the nucleon EMT form factors [26, 27], on the other hand, we do not encounter such a complexity [28], since such a Lorentz boost factor m/E does not appear fortuitously. Thus, we can directly connect the 3D BF distributions of the EMT form factors to the 2D IMF densities without any technical problems for the nucleon. Furthermore, if we consider both the EM and EMT form factors for the higher-spin particle, the relativistic effects raise similar problems in a more complicated manner [14, 45]. In the present work, we thus carry out the Abel transformation in projecting the 3D BF distributions to the 2D BF densities instead of the 2D IMF ones.

The Abel transformation and its inverse transformation are defined as

$$A[g](x_\perp) = \mathcal{G}(x_\perp) = \int_{x_\perp}^{\infty} \frac{dr}{r} \frac{g(r)}{\sqrt{r^2 - x_\perp^2}}, \quad g(r) = -\frac{2}{\pi} r^2 \int_r^{\infty} dx_\perp \frac{d\mathcal{G}(x_\perp)}{dx_\perp} \frac{g(r)}{\sqrt{x_\perp^2 - r^2}}. \tag{68}$$

$\mathcal{G}(b)$ is called the Abel image of the function $g(r)$. For example, if there is no higher multipole distribution in the BF, the Abel image of the monopole mass distribution is found to be

$$\int dx_z \langle \hat{T}^{00}(0) \rangle_{-r, \mathbf{0}} = \int dx_z \varepsilon_0(r) \delta_{\lambda'\lambda} = \varepsilon_0^{(2D)}(x_\perp) \delta_{\lambda'\lambda}, \quad \varepsilon_0^{(2D)}(x_\perp) = \int_{x_\perp}^{\infty} dr \frac{2r\varepsilon_0(r)}{\sqrt{r^2 - x_\perp^2}}. \tag{69}$$

The Abel transformation can be straightforwardly applied to the nucleon and the pion, since they do not have any quadrupole distributions. However, as we pointed out in Ref. [14], mapping the 3D distribution onto the 2D one in the presence of the quadrupole structure brings about additional contributions. Collecting all the angle-dependent Abel images in 3D space, we are able to reconstruct them in 2D space. It has been already discussed in various contexts [46–49]. While the single Abel image is enough for a spherically symmetric distribution, the angle-dependent distribution requires more than one Abel image [50]. The scanning in all directions are required to project angle-dependent 3D distributions to 2D ones in general. In fact, the number of the scans depends on the shape of the distributions [47]. In our case, we need two Abel images only, which is a very special case of the anisotropic distributions. To generalize them, we should introduce the Radon transformation [51]. The Abel transformation we keep using is just a special case of the Radon transformation and is deeply related to it [48, 49]. In the present case, we need to integrate $\varepsilon(r) Y^{ij}(\Omega_r)$ over the z -axis for each 3D angle. The angle-dependent Abel transformation can be analytically achieved as follows:

$$\int dx_z \varepsilon_2(r) Y^{ij}(\Omega_r) \hat{Q}_{\lambda'\lambda}^{ij} = \varepsilon_2^{(2D)}(x_\perp) X_2^{ij}(\theta_{x_\perp}) \hat{Q}^{ij} + \Delta_\varepsilon(x_\perp) \left(-\frac{1}{3} \delta_{\sigma'\sigma} + \frac{2}{3} \delta_{\lambda'3} \delta_{3\lambda} \right), \tag{70}$$

with

$$\varepsilon_2^{(2D)}(x_\perp) = \int_{x_\perp}^{\infty} dr \frac{2x_\perp^2 \varepsilon_2(r)}{r \sqrt{r^2 - x_\perp^2}}, \quad \Delta_\varepsilon(x_\perp) = \int_{x_\perp}^{\infty} dr \frac{(3x_\perp^2 - 2r^2) \varepsilon_2(r)}{r \sqrt{r^2 - x_\perp^2}}. \quad (71)$$

Employing the above expression, we derive the explicit connections between the 2D and 3D distributions in the BF by the Abel transformations

$$\varepsilon_{(0,0)}^{(2D)}(x_\perp) + 2\varepsilon_{(0,1)}^{(2D)}(x_\perp) = 6 \int_{x_\perp}^{\infty} \frac{r dr}{\sqrt{r^2 - x_\perp^2}} \varepsilon_0(r) = 3\varepsilon_0^{(2D)}(x_\perp), \quad (72)$$

$$\Delta_\varepsilon(x_\perp) := \varepsilon_{(0,0)}^{(2D)}(x_\perp) - \varepsilon_{(0,1)}^{(2D)}(x_\perp) = -\frac{\partial_{(2D)}^2}{4m} \tilde{\mathcal{E}}_2(x_\perp), \quad (73)$$

Under this transformation, we observe that the rank-2 irreducible tensor in 3D space is reduced to the rank-2 irreducible tensor in 2D space and a part of the diagonal contributions leaks out to the rank-0 irreducible tensor in the 2D space. This *induced monopole* distribution Δ_ε is responsible for the splitting of the mass distributions with the longitudinally and transversely polarized spins. Note that the 2D spin distributions of the nucleon were intensively discussed in Refs. [27, 52, 53].

The nucleon monopole pressure and shear forces were investigated in Ref. [26, 27] by means of the Abel transformation. When it comes to a non-spherical hadron, all the quadrupole pressure and shear force distributions are connected to each other via the Abel transformation in the same manner:

$$p_n^{(2D)}(x_\perp) + \frac{1}{2}s_n^{(2D)}(x_\perp) = \int_{x_\perp}^{\infty} \frac{r dr}{\sqrt{r^2 - x_\perp^2}} \left(p_n(r) + \frac{2}{3}s_n(r) \right),$$

$$s_n^{(2D)}(x_\perp) = 2 \int_{x_\perp}^{\infty} \frac{x_\perp^2 dr}{r \sqrt{r^2 - x_\perp^2}} s_n(r). \quad (74)$$

Note that the definitions of the pressure and shear forces are different from those in Ref. [26] by factor 1/2.

V. NUMERICAL RESULTS AND DISCUSSION

Since we want to investigate the general features of the mechanical structure of the spin-1 particle, we will not use a specific model but employ a simplified toy model for the GFFs. We utilize the simple multipole parametrization for the t dependence. The mass and spin form factors are normalized to be 1 at $t = 0$. The quadrupole mass form factor at $t = 0$ is also taken to be 1. On the other hand, the values of the D -term form factors at $t = 0$ are unknown. To determine them, we need results from models (see for example Refs. [34, 54]). However, we take arbitrary negative values for the constant D -terms at $t = 0$, assuming that their negative values impose the stability conditions on the spin-1 particle. As observed in Eq. (17), the kinematical factor τ enters in the expressions for the GFFs in the IMF. This means that when we carry out the inverse 2D Fourier transforms to obtain the EMT densities in the IMF, τ may cause the divergence. While this may have a physical meaning as in the case of the pion, we do not know if this is the case also for the spin-1 particle. In the current work, we will assume that the EMT densities do not have any singular behavior. So, we parametrize the GFFs by using generically the following quadrupole type of the parametrization:

$$G(t) = \frac{G(0)}{(1 - t/\Lambda^2)^4}. \quad (75)$$

Here, we introduce the cutoff value $\Lambda = 2m_\rho$, where m_ρ is the ρ -meson mass. The values of $\mathcal{D}_n(0)$ are taken to be $\mathcal{D}_0(0) = \mathcal{D}_2(0) = \mathcal{D}_3(0) = -1$. Since the values of all the D -term form factors are taken to be the same, we have the same values of $p_n(x_\perp)$ and $s_n(x_\perp)$ in the 2D BF. This choice of D -term values yields merit that we can comprehensively examine the relativistic effects when we move from the 2D BF to the 2D IMF, as will be observed later.

A. Mass distributions in the 2D transverse plane

The mass distributions in the 2D BF can be obtained by the Abel transformation of those in the 3D BF, as shown in Eqs. (69) and (70). The Abel transformation of the quadrupole mass distribution in the 3D BF, $\varepsilon_2(r)$, yields the

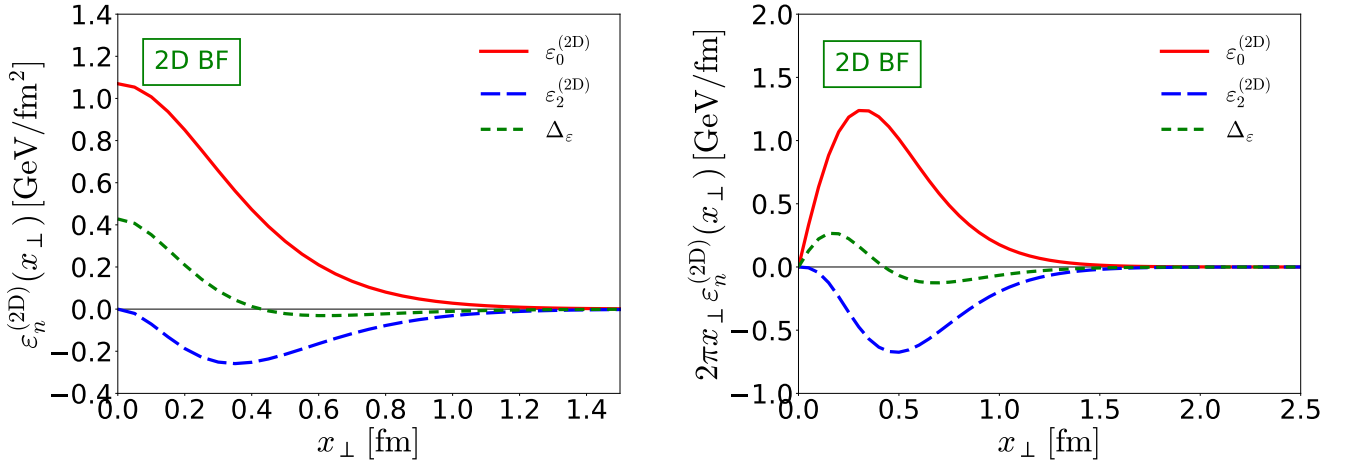


FIG. 1. Mass distributions of a spin-1 particle in the 2D Breit frame. In the left panel, the solid, dashed, and short-dashed curves draw the numerical results for $\varepsilon_0^{(2D)}$, $\varepsilon_2^{(2D)}$, and Δ_ε defined in Eq. (69) and Eq. (72), respectively. In the right panel, those weighted by $2\pi x_\perp$ are exhibited.

induced monopole distribution $\Delta_\varepsilon(x_\perp)$. Thus, we have three different terms for the mass distributions in the 2D BF: $\varepsilon_0(x_\perp)$, $\Delta_\varepsilon(x_\perp)$, and $\varepsilon_2(x_\perp)$. We draw the numerical results for them in Fig. 1. The monopole mass distribution is dominant over the induced monopole and quadrupole ones. The quadrupole mass density is negative in the whole region of x_\perp whereas the induced monopole mass distribution, $\Delta_\varepsilon(x_\perp)$, is positive till it reaches around 0.4 fm and then turns negative. As shown in Eqs. (72) and (73), $\varepsilon_{(0,0)}^{(2D)}$ and $\varepsilon_{(0,1)}^{(2D)}$ can be expressed in terms of $\varepsilon_0^{(2D)}$ and Δ_ε :

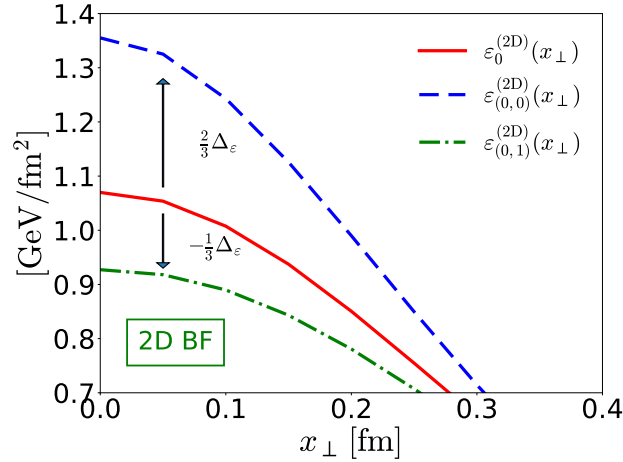


FIG. 2. Mass densities of a spin-1 particle in the 2D Breit frame. The solid, dashed, and dot-dashed curves show the numerical results for $\varepsilon_0^{(2D)}$, $\varepsilon_{(0,0)}^{(2D)}$, and $\varepsilon_{(0,1)}^{(2D)}$. Δ_ε is defined in Eq. (73).

$$\varepsilon_{(0,0)}^{(2D)}(x_\perp) = \varepsilon_0^{(2D)}(x_\perp) + \frac{2}{3}\Delta_\varepsilon(x_\perp), \quad \varepsilon_{(0,1)}^{(2D)}(x_\perp) = \varepsilon_0^{(2D)}(x_\perp) - \frac{1}{3}\Delta_\varepsilon(x_\perp). \quad (76)$$

Thus, $\varepsilon_{(0,0)}^{(2D)}$ and $\varepsilon_{(0,1)}^{(2D)}$ are split by Δ_ε as shown in Fig. 2. It indicates that the magnitude of $\varepsilon_{(0,0)}^{(2D)}$ is larger than $\varepsilon_{(0,1)}^{(2D)}$. Since the contribution of the inner part of the nodal point cancels out that of the outer part, Δ_ε does not affect the normalization of the mass as shown in the following integration

$$\int d^2x_\perp \Delta_\varepsilon(x_\perp) = - \int d^2x_\perp \frac{\partial_{(2D)}^2 \tilde{\mathcal{E}}_2(x_\perp)}{4m} = 0. \quad (77)$$

The induced monopole mass distribution changes only the shape of the mass distribution.

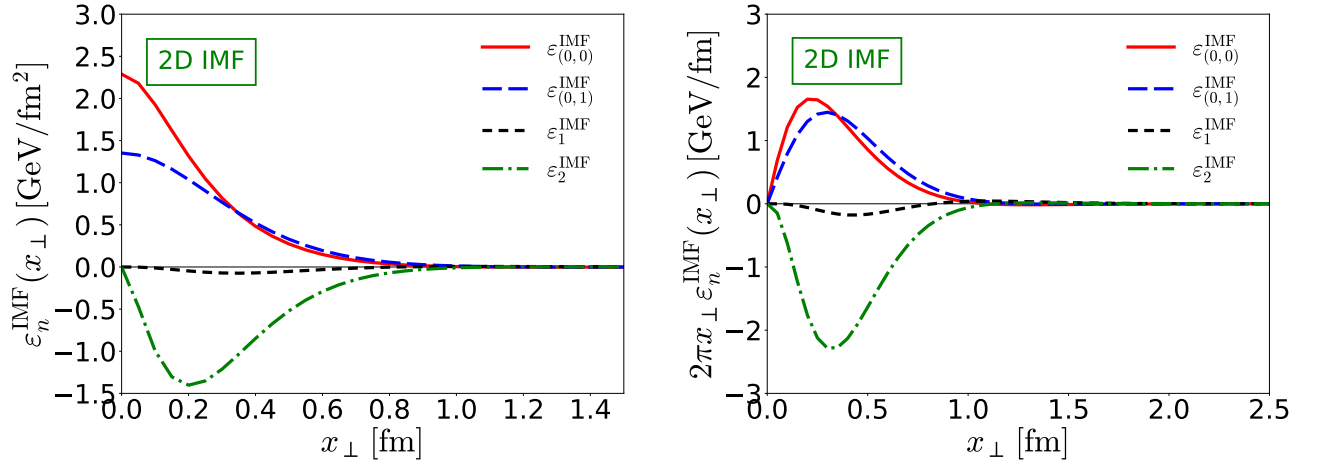


FIG. 3. Transverse mass densities of a spin-1 particle in the 2D infinite-momentum frame. The solid and dashed curves draw the 2D mass densities $\varepsilon_{(0,0)}^{\text{IMF}}$ and $\varepsilon_{(0,1)}^{\text{IMF}}$, whereas the short-dashed and dot-dashed ones depict $\varepsilon_1^{\text{IMF}}$ and $\varepsilon_2^{\text{IMF}}$. The expressions for these mass densities are given in Eq. (54). In the right panel, we draw those weighted by $2\pi x_\perp$.

Figure 3 depicts the transverse mass densities in the 2D IMF. We have the following relations:

$$\varepsilon_{(0,0)}^{\text{IMF}}(x_\perp) > 0, \quad \varepsilon_{(0,1)}^{\text{IMF}}(x_\perp) > 0. \quad (78)$$

The induced transverse dipole mass density is much smaller than the other transverse mass densities. Note that $\varepsilon_1^{\text{IMF}}(x_\perp)$ and $\varepsilon_2^{\text{IMF}}(x_\perp)$ vanish at $x_\perp = 0$. As discussed in the previous section, the integral of the x_\perp -weighted induced dipole mass density over x_\perp vanishes:

$$\int d^2x_\perp x_\perp \varepsilon_1^{\text{IMF}}(x_\perp) = 0. \quad (79)$$

Note that this condition is highly nontrivial. The right panel depicts the mass distributions weighted by $2\pi x_\perp$.

It is of great use to visualize the 2D mass distributions for the polarized spin-1 particle, so that we can see how its mass is distributed and influenced under the polarization. As shown explicitly in Appendix B, we can derive the expressions for the mass distribution in the 2D BF by choosing specifically the polarization. In Fig. 4, we draw $T_{\text{EF}}^{00}(\mathbf{x}_\perp, 0, \lambda', \lambda)$ by choosing four different polarizations. The upper-left panel of Fig. 4 illustrates the mass distribution of the spin-1 particle with $s_x = 1$ when it is polarized along the x axis. As written in Eq. (B12), the mass distribution contains all contributions. The quadrupole term $\cos 2\theta \varepsilon_2^{(2D)}(x_\perp)/4$ introduces the angular dependence of the mass distribution. As shown in Fig. 1, the quadrupole term is negative over the whole region in the 2D BF. Putting them together, we observe that the mass distribution in the 2D BF is squeezed into a 2D prolate form. On the other hand, when the spin-1 particle is polarized along the x -axis with $s_x = 0$ chosen, the scalar term $\varepsilon_{(0,0)}^{(2D)}(x_\perp)$ vanishes, so that we have only two different contributions, i.e., $\varepsilon_{(0,1)}^{(2D)}$ and $-\cos 2\theta \varepsilon_2^{(2D)}/2$ as given in Eq. (B11). Since we have already shown in Fig. 3 that $\varepsilon_{(0,1)}^{(2D)}$ is smaller than $\varepsilon_{(0,0)}^{(2D)}$ and we have a larger positive quadrupole contribution to the mass distribution, compared to the previous case ($s_x = 1$), we expect that the mass distribution should be compressed along the y -axis. Thus, its shape becomes oblate as shown in the upper-right panel of Fig. 4. When the spin-1 particle is polarized along the z -axis, the scalar contribution survives only regardless of choosing a specific value of s_z . Thus, the mass distribution of the spin-1 particle polarized along the z -axis is always in a spherical shape, as visualized in the lower panel of Fig. 4.

We now consider the mass distribution of the spin-1 particle in the 2D IMF. As written in Eq. (53), it acquires the induced dipole contribution that arises from the Lorentz boost. We have presented its explicit expressions in Eq. (B16) given in Appendix B when the polarization of the spin-1 particle is fixed. In addition to the quadrupole contribution, the induced dipole one provides an additional angular dependence of the mass distribution. Thus, when the spin-1 particle is polarized along the x -axis with $s_x = 1$, the mass distribution is contracted to be prolate, which is similar to that in the 2D BF. However, we can observe a clear signature of the dipole feature when the spin-1 particle is polarized along $s_x = 1$, as drawn in the upper-left panel of Fig. 5. The upper-right panel displays the clear quadrupole structure. It indicates that the Lorentz boost intensifies the quadrupole pattern. When the spin-1 particle is polarized along the z -axis, only the scalar contribution survives as in the case of the mass distribution in the 2D BF.

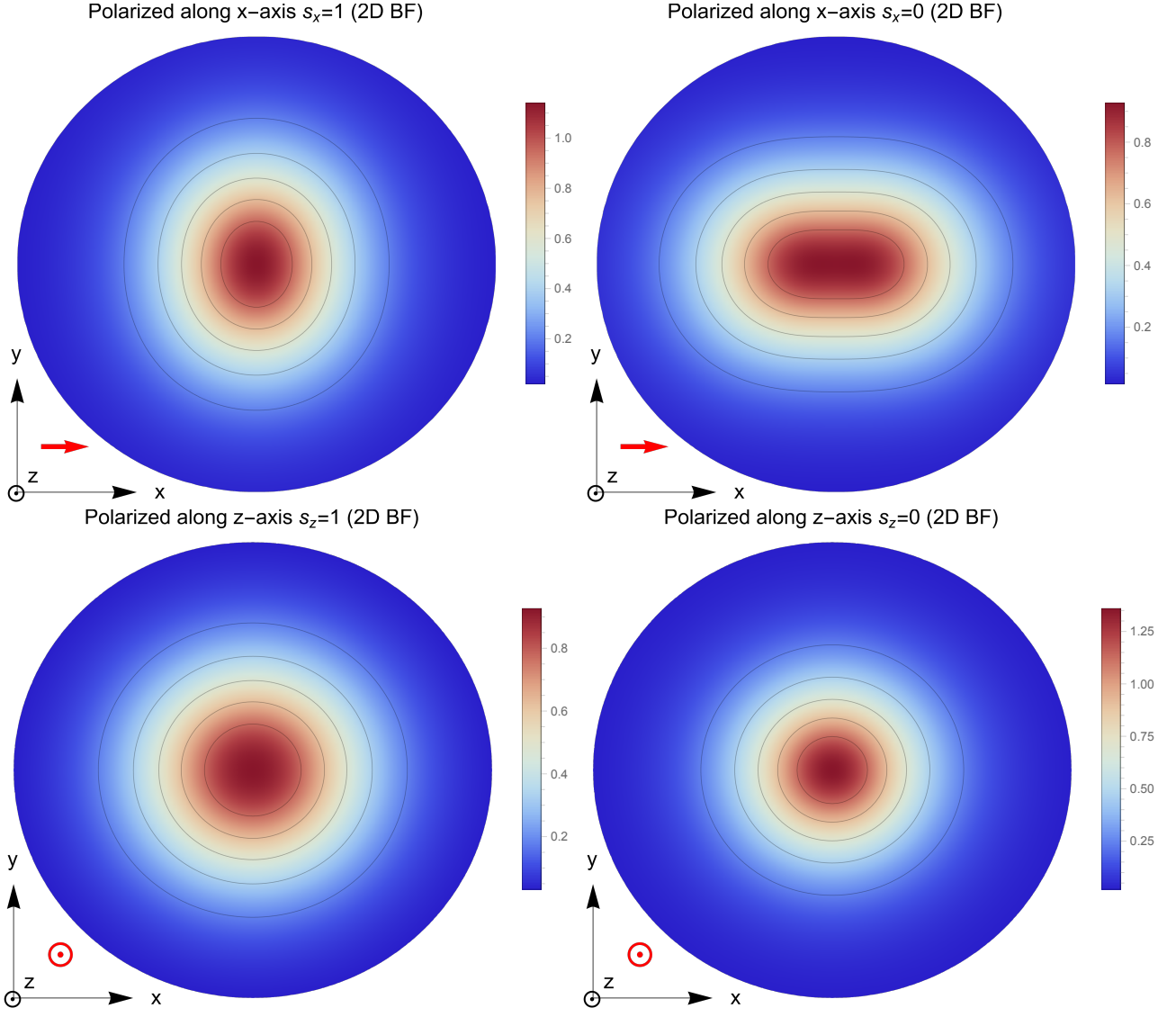


FIG. 4. $T^{00}(x_{\perp})$ visualized in the 2D BF by choosing a specific polarization. In the upper-left (upper-right) panel, we draw the mass distribution when the spin-1 particle is polarized with $s_x = 1$ ($s_x = 0$). In the lower-left (lower-right) panel, we illustrate that with $s_z = 1$ ($s_z = 0$).

B. Mechanical properties of a spin-1 particle

We are now in a position to discuss the mechanical properties of a spin-1 particle. The 3D pressure and shear-force densities can be derived by the inverse Fourier transformation as given in Eqs. (34) and (33). Transforming the derived 3D BF pressure and shear-force distributions by the Abel transformation, we obtain those in the 2D BF. Since we employ the same form for the GFFs of the spin-1 particle, the pressure and shear-force distributions become degenerate respectively for all n , as shown in Fig. 6. This degenerate forms of p_n and s_n have a virtue that the relativistic effects can clearly emerge when the longitudinal momentum of the spin-1 particle goes to infinity.

When the spin-1 particle is boosted by the Lorentz transformation, the p_n and s_n distributions undergo drastic changes. So, the pressure and shear-force densities in the 2D IMF reveal the relativistic effects as exhibited in Fig. 7. We observe that the degeneracy imposed on the pressure and shear-force distributions are removed. As mentioned previously, p_1^{IMF} and s_1^{IMF} arise from the Lorentz boost. The pressure densities satisfy the stability condition as in Eq. (64). This indicates that the pressure densities in the 2D IMF should have the odd number of the nodal points. As shown in the lower-left panel, we depict the pressure densities weighted by $2\pi x_{\perp}$. $p_{(0,1)}^{\text{IMF}}$ has three nodal points whereas all other pressure densities have only one as those in the 2D BF. It is interesting to see that the newly

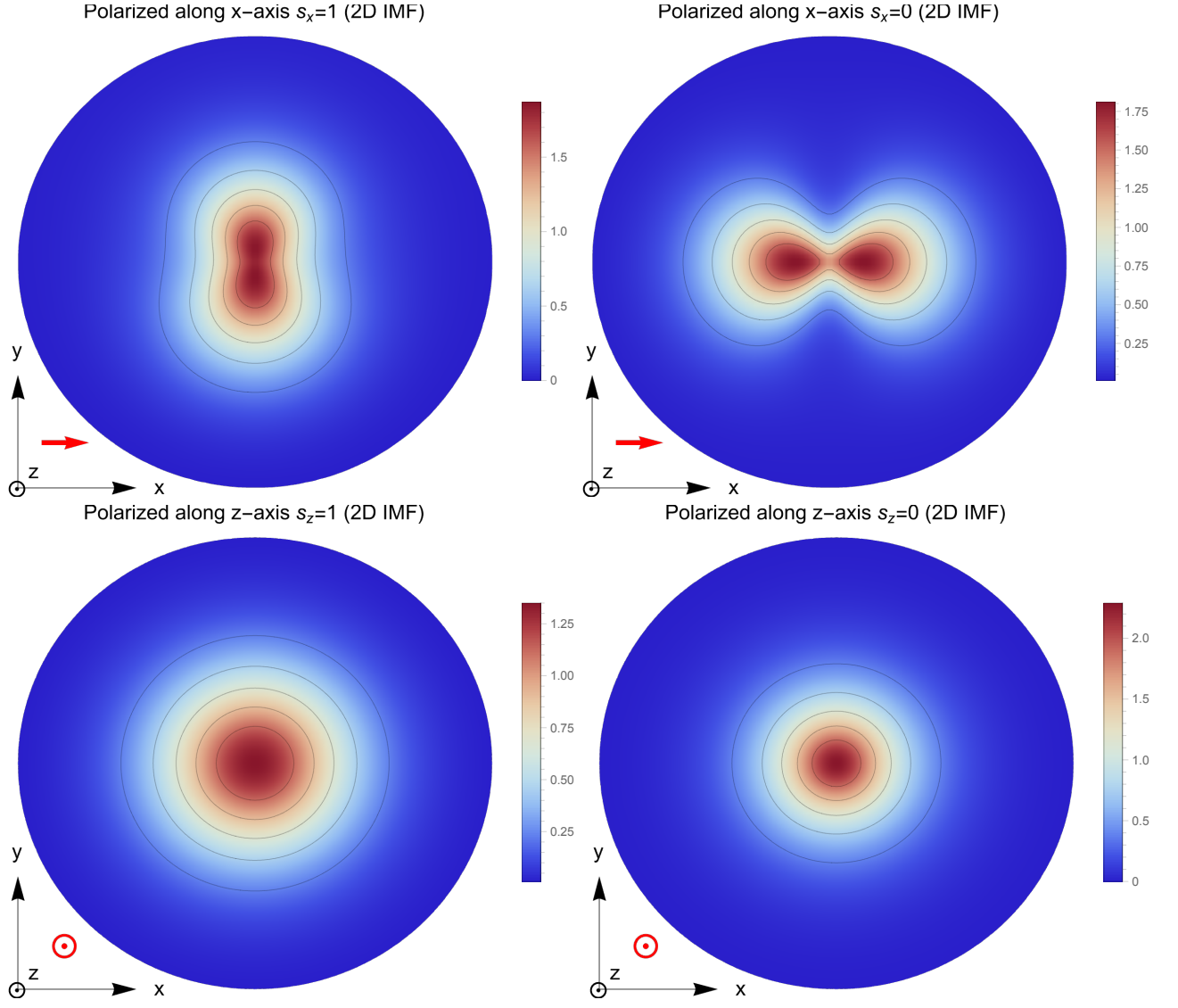


FIG. 5. $T^{00}(x_{\perp})$ visualized in the 2D IMF by choosing a specific polarization. In the upper-left (upper-right) panel, we draw the mass distribution when the spin-1 particle is polarized with $s_x = 1$ ($s_x = 0$). In the lower-left (lower-right) panel, we illustrate that with $s_z = 1$ ($s_z = 0$).

emerged induced pressure p_1^{IMF} under Lorentz boost is negative at the center in contrast to other pressures. The shear-force densities in the 2D IMF also exhibit interesting features. As shown in Fig. 6, the shear-force distributions are all positive and degenerate. When the momentum of the spin-1 particle becomes infinite, all the components of the shear-force densities come apart. The sign of $s_1^{\text{IMF}}(x_{\perp})$ becomes even negative. The negative features of the pressure and shear-force densities are related to the positive D -term in the IMF (19), which originates from the solely relativistic effects. More interestingly, $s_{(0,1)}^{\text{IMF}}$ has two nodal points. These are unique features for the spin-1 particle and higher spin states.

In Figs. 8 and 9, we illustrate the strong force fields inside a spin-1 at rest and in the fast-moving frame, respectively, when it is polarized along the x -axis (upper panel) and z -axis (lower panel). In Appendix C, we have explicitly written the expressions for the strong force fields with the direction of the polarization chosen. In the 2D IMF, we observe the dipole pattern in the upper-left panel and the quadrupole structure in the upper-right panel as in the mass distributions. Note that the strong force fields shown in Figs. 8 and 9 consist of partial ones. If one considers all the force fields, they vanish at each local point. In other words, the energy and momentum flow in both directions along the arrows in Figs. 8 and 9, so that the net flows vanish. For simplicity, we present only one direction indicated by the arrows. Nevertheless, the strong force fields visualized in Figs. 8 and 9 exhibit how the relativistic effects change the behavior of the strong force fields inside a spin-1 particle.

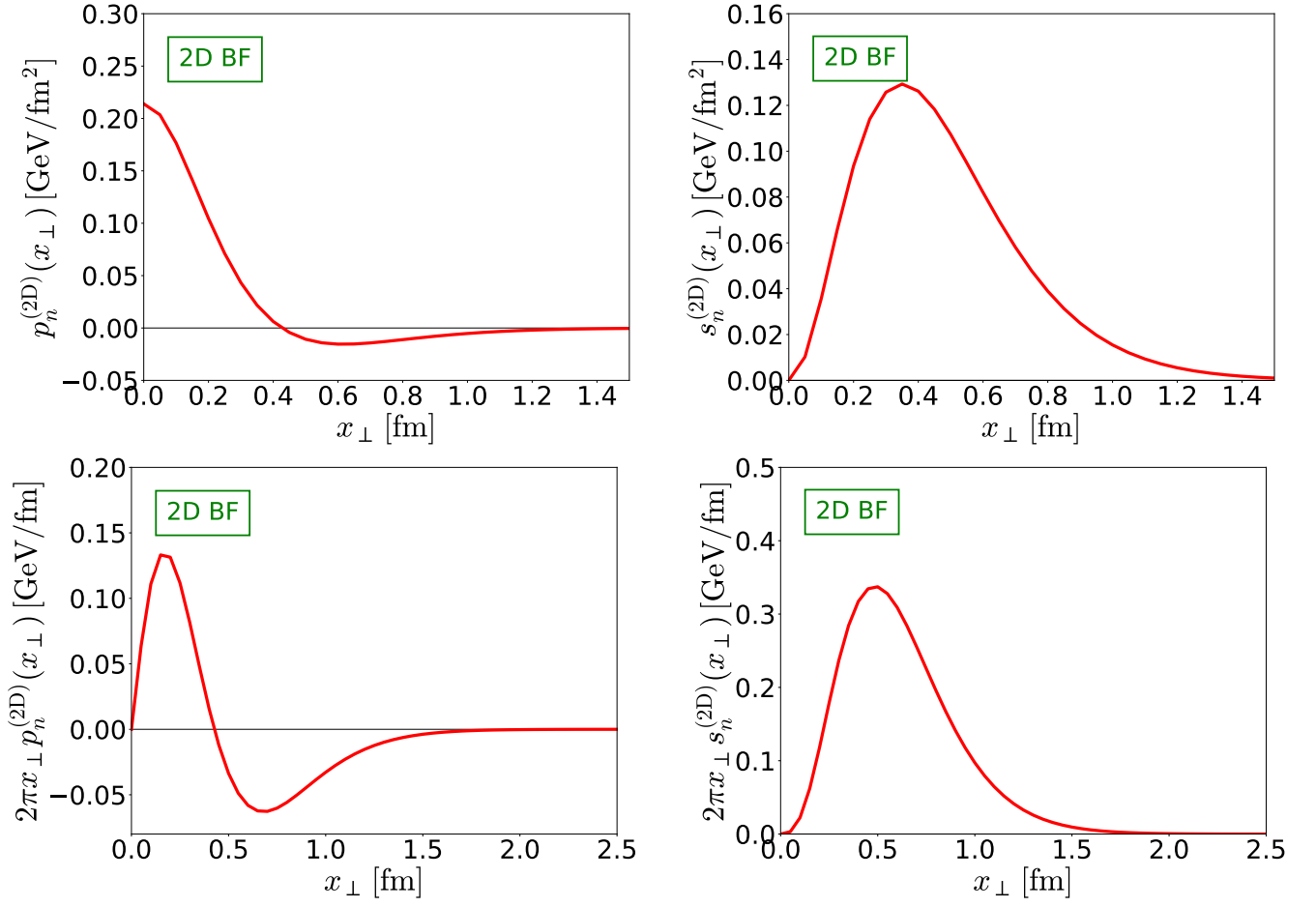


FIG. 6. Pressure and shear-force distributions ($p_n^{(2D)}$ and $s_n^{(2D)}$) in the 2D BF. In the lower panel, we draw those weighted by $2\pi x_\perp$.

As written in Eq. (51), the strong force fields in the 2D BF have only the monopole and quadrupole terms. Thus, when the spin-1 particle is polarized along the x -axis with both $s_x = 1$ and $s_x = 0$, the quadrupole patterns are seen as in the upper panel of Fig. 8. When it is polarized along the z -axis, we find only the monopole pattern. On the other hand, the Lorentz boost induces the dipole term in the spatial component of the EMT densities (see Eq. (60)). When the spin-1 particle is polarized along the x -axis with $s_x = 1$ chosen, all the dipole and quadrupole terms contribute to the strong force fields as shown in Eq. (C8). The upper-left panel of Fig. 9 reveals clearly this feature. However, if one selects $s_x = 0$ with the spin-1 particle polarized along the x -axis, all the dipole contributions vanish. So, the upper-right panel of Fig. 9 demonstrates the quadrupole pattern, being similar to that in the 2D BF. When the spin-1 particle is polarized along the z -axis, the strong force fields in the 2D IMF are not much different from those in the 2D BF. These features of the strong force fields resemble the mass 2D distributions.

VI. SUMMARY AND CONCLUSIONS

In the present work, we scrutinized the mechanical structure of the spin-1 particle. We first formulated the gravitational form factors and the energy-momentum tensor distributions in three different frames: the three-dimensional Breit frame, the two-dimensional Breit frame, and the two-dimensional infinite-momentum frame (or equivalently the Drell-Yan frame). By introducing these three different frames, we were able to distinguish the geometric effects from the relativistic effects that arise from the Lorentz boost. A prominent point is that an additional monopole structure is induced by going from the three-dimensional Breit frame to the two-dimensional one. This can be achieved by the Abel transformation. The two-dimensional infinite-momentum frame can be reached by taking the limit of the infinite longitudinal momentum of the spin-1 particle. This Lorentz boost induces the dipole mass density, of which the integration over the transverse plane vanishes because of the normalization of the mass and spin of the spin-1

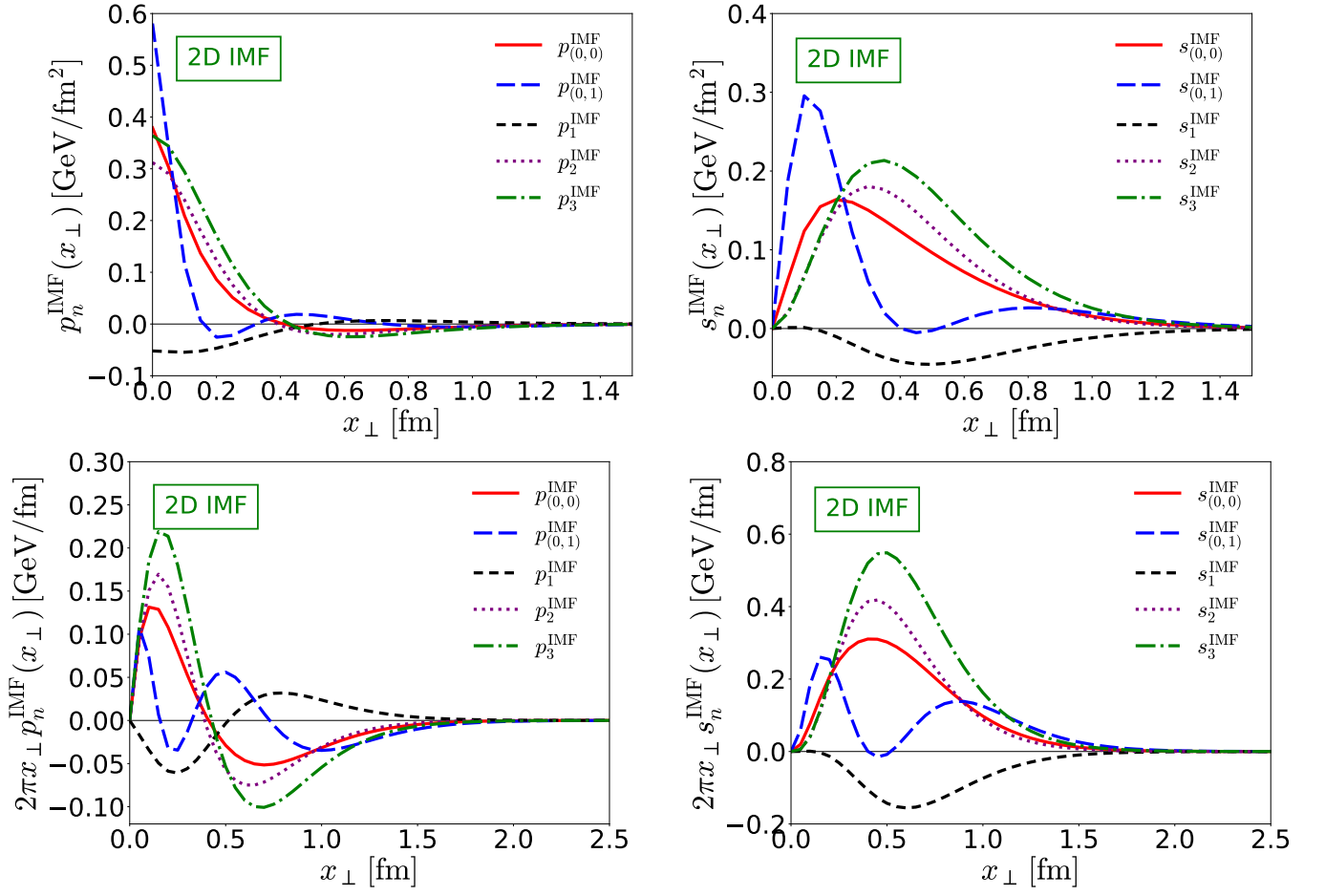


FIG. 7. Pressure and shear-force densities in the 2D IMF. In the lower panel, we draw those weighted by $2\pi x_{\perp}$. The decomposition of the pressure and shear-force densities are defined in Eq. (60).

particle. This provides a nontrivial constraint on the induced dipole mass density. When the spin-1 particle is polarized along the x -axis with $s_x = 1$, the mass distribution reveals the quadrupole pattern in the two-dimensional Breit frame. When its momentum goes to infinity, the induced dipole mass is generated, so that one can clearly observe the dipole pattern in the mass density. When the spin state of the spin-1 particle is taken to be $s_x = 0$, the quadrupole structure is enhanced by the Lorentz boost.

The relativistic effects on the pressure and shear-force densities are even more prominent. Since we take the same quadratic form of the gravitational form factors, the pressure and shear-force distributions become degenerate regardless of the value of the subscript n . However, when we go from the two-dimensional Breit frame to the two-dimensional infinite momentum frame, the pressure and shear-force densities undergo drastic changes. While the pressure distributions in the two-dimensional Breit frame have only one nodal point, which is essential for them to satisfy the stability conditions, $p_{(0,1)}^{\text{IMF}}$ has even three nodal points because of the Lorentz boost. Interestingly, the sign of p_1^{IMF} becomes negative in the core part in contrast to the any other pressures. The shear-force densities also exhibit unique features under the Lorentz boost. $s_{(0,1)}^{\text{IMF}}$ has two nodal points and s_1^{IMF} becomes negative. The negative values of the pressure and shear-force densities are related to the positive D -term in the IMF, which arises from the solely relativistic effects. We also visualized the strong force fields inside a spin-1 particle. Though they vanish at each local point, they display the multipole structure of the spin-1 particle, in particular, when it is polarized along the x -axis. The most interesting behavior of the strong force fields can be found by choosing $s_x = 1$. In this case, all the dipole and quadrupole terms contribute to the strong force fields.

In the current work, we focused on the mechanical structure of a generic spin-1 particle. However, we want to mention that there are several spin-1 particles such as the ρ meson, the ω meson, the vector kaon, the a_1 meson, and the deuteron. While they share the general features discussed in the present work, they will possibly show quantitative differences each other. In particular, the deuteron can be treated as a non-relativistic particle, whereas all the vector

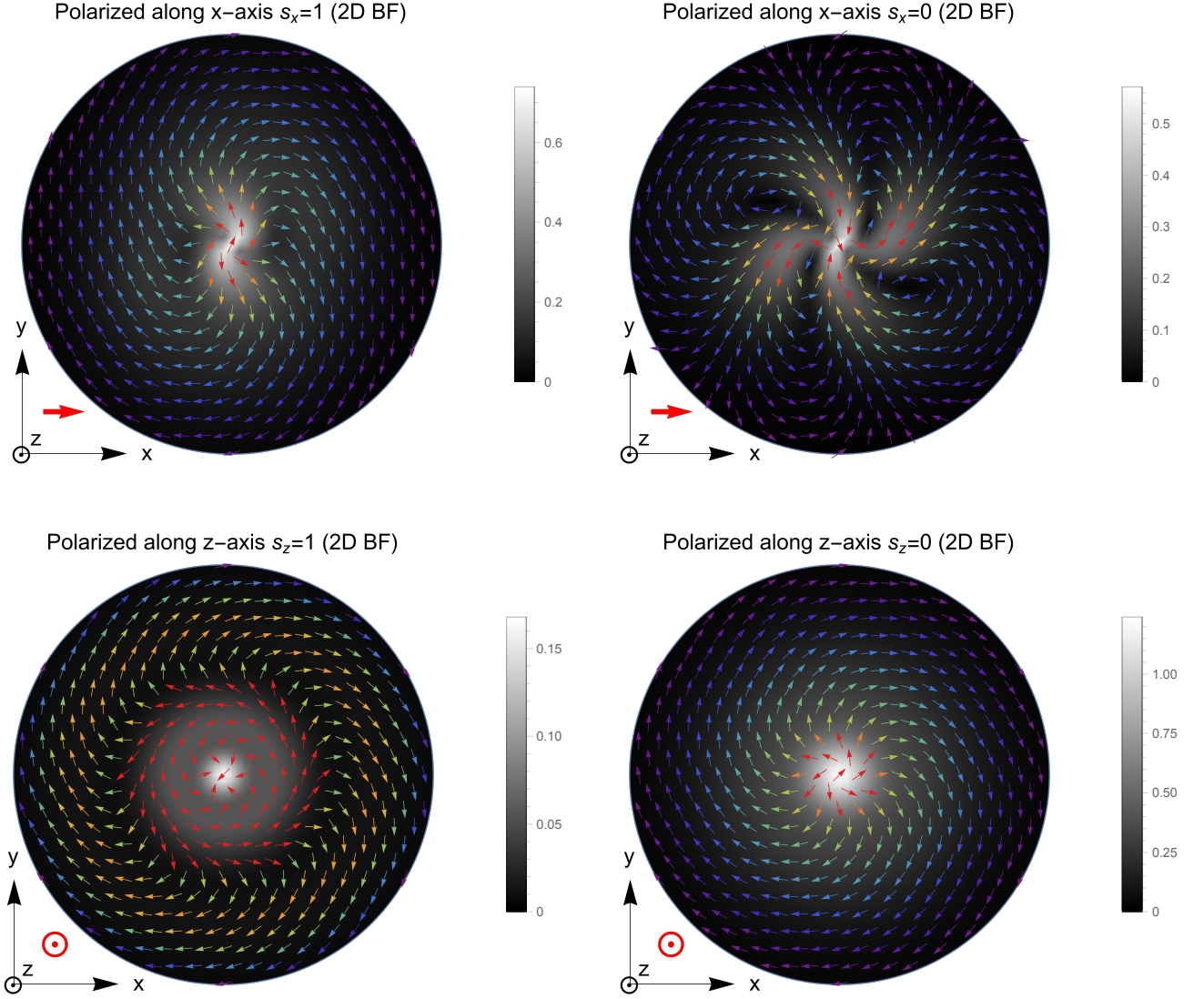


FIG. 8. Strong force fields inside a spin-1 particle in the rest frame ($P_z = 0$) are visualized in the 2D plane when the target is polarized along x - and z -axis.

mesons should be considered as relativistic ones. Apart from the relativistic effects, there may be certain effects due to the different quark configuration of the vector mesons. The corresponding study will appear elsewhere.

ACKNOWLEDGMENTS

Authors want to express their gratitude to C.Lorcé for invaluable comments and criticism. J.-Y.K. is supported by the Deutscher Akademischer Austauschdienst(DAAD) doctoral scholarship. The work of H.-Ch.K. was supported by Basic Science Research Program through the National Research Foundation of Korea funded by the Korean government (Ministry of Education, Science and Technology, MEST), Grant-No. 2021R1A2C2093368 and 2018R1A5A1025563. The work of B.-D.S. is supported by Guangdong Provincial funding with Grant No. 2019QN01X172, the National Natural Science Foundation of China with Grant No. 12035007 and No. 11947228, Guangdong Major Project of Basic and Applied Basic Research No. 2020B0301030008, and the Department of Science and Technology of Guangdong Province with Grant No. 2022A0505030010.

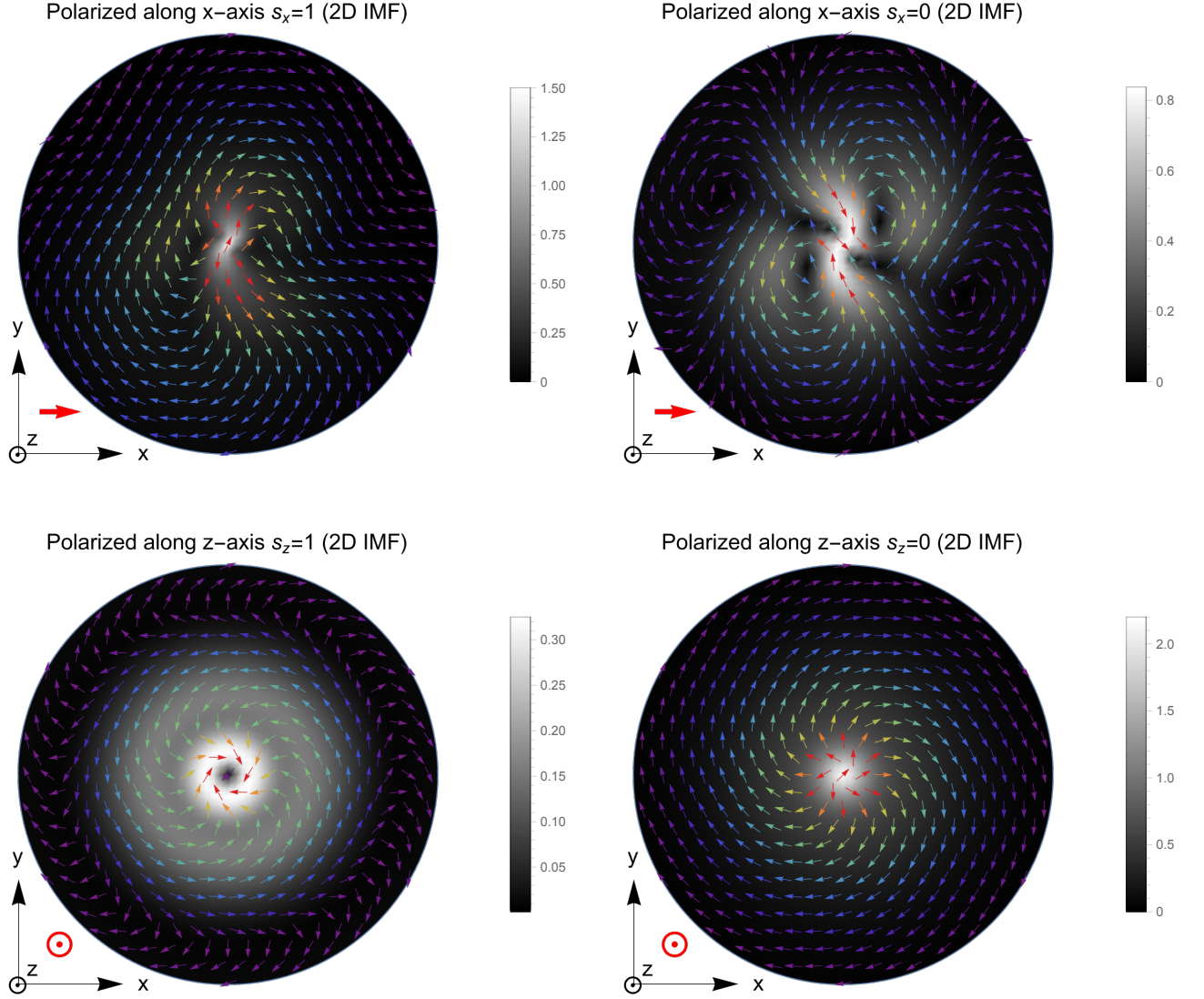


FIG. 9. Strong force fields inside a fastly moving spi-1 particle ($P_z = \infty$) are visualized in the 2D plane when the target is polarized along x - and z -axis.

Appendix A: Gravitational form factors of a spin-1 particle in the two-dimensional Drell-Yan frame

The results from the light-front formalism should coincide with the those from the IMF. As a cross-check, we are able to carry out the same calculation in the light-front formalism. A light-front four-vector is given by

$$x^\nu = \{x^+, x^-, \mathbf{x}_\perp\}, \quad (\text{A1})$$

with $x^\pm = (x^0 \pm x^3)/\sqrt{2}$. The Drell-Yan frame is defined by $\Delta^+ = 0$. The kinematics are given by

$$P = \frac{1}{2}(p' + p) = (P^+, P^-, \mathbf{0}), \quad \Delta = (p' - p) = (0, 0, \mathbf{\Delta}_\perp), \quad \text{with } P^- = \frac{1}{2P^+} \left(m^2 + \frac{\mathbf{\Delta}_\perp^2}{4} \right). \quad (\text{A2})$$

The matrix elements of T^{++} , T^{+i} , and T^{ij} are respectively decomposed in terms of the gravitational form factors as follows:

$$\begin{aligned}
\langle p', \lambda' | T^{++}(0) | p, \lambda \rangle &= 2P^{+2} \mathcal{E}_{(0,0)}^{\text{IMF}}(t) \delta_{\lambda'3} \delta_{3\lambda} + 2P^{+2} \mathcal{E}_{(0,1)}^{\text{IMF}}(t) \delta_{\sigma'\sigma} \\
&\quad + 2P^{+2} \sqrt{\tau} \mathcal{E}_1^{\text{IMF}}(t) i \epsilon^{3jk} \hat{S}_{\lambda'\lambda}^j X_1^k(\theta_{\Delta_\perp}) + 4P^{+2} \tau \mathcal{E}_2^{\text{IMF}}(t) \hat{Q}^{kl} X_2^{kl}(\theta_{\Delta_\perp}), \\
\langle p', \lambda' | T^{+i}(0) | p, \lambda \rangle &= 2mP^+ \sqrt{\tau} i \epsilon^{3li} \hat{S}_{\lambda'\lambda}^3 X_1^l(\theta_{\Delta_\perp}) \mathcal{J}_1^{\text{IMF}}(t) + 4mP^+ \tau \left(X_2^{ik}(\theta_{\Delta_\perp}) - \frac{1}{2} \delta^{ik} \right) \mathcal{J}_2^{\text{IMF}}(t) \hat{Q}^{3k}, \\
\langle p', \lambda' | T^{ij}(0) | p, \lambda \rangle &= 2m^2 \tau \left[\left(\frac{1}{3} \mathcal{D}_2^{\text{IMF}} - \frac{1}{2} \mathcal{D}_{(0,1)}^{\text{IMF}} \right) \delta_{\sigma'\sigma} + \left(-\frac{2}{3} \mathcal{D}_2^{\text{IMF}} - \frac{1}{2} \mathcal{D}_{(0,0)}^{\text{IMF}} \right) \delta_{\lambda'3} \delta_{\lambda 3} \right] \delta^{ij} \\
&\quad + 2m^2 \tau X_2^{ij}(\theta_{\Delta_\perp}) \left[\delta_{\sigma'\sigma} \mathcal{D}_{(0,1)}^{\text{IMF}}(t) + \delta_{\lambda'3} \delta_{\lambda 3} \mathcal{D}_{(0,0)}^{\text{IMF}}(t) \right] \\
&\quad + 4m^2 \tau \left[\hat{Q}^{ik} X_2^{jk}(\theta_{\Delta_\perp}) + \hat{Q}^{jk} X_2^{ik}(\theta_{\Delta_\perp}) - \hat{Q}^{lm} X_2^{lm}(\theta_{\Delta_\perp}) \delta^{ij} \right] \mathcal{D}_2^{\text{IMF}}(t) \\
&\quad + 8m^2 \tau^{3/2} i \epsilon^{lm3} \hat{S}^l X_1^m(\theta_{\Delta_\perp}) \left(X_2^{ij}(\theta_{\Delta_\perp}) - \frac{1}{2} \delta^{ij} \right) \mathcal{D}_1^{\text{IMF}}(t) \\
&\quad + 8m^2 \tau^2 \hat{Q}^{lm} \left(X_2^{lm}(\theta_{\Delta_\perp}) + \frac{1}{2} \delta^{lm} \right) \left(X_2^{ij}(\theta_{\Delta_\perp}) - \frac{1}{2} \delta^{ij} \right) \mathcal{D}_3^{\text{IMF}}(t). \tag{A3}
\end{aligned}$$

The decompositions in Eq. (A3) are identical to those in the infinite momentum frame.

Appendix B: Explicit calculation of the mass distributions

Since the basis used in this work is not a standard one, we first provide the conversion from the current basis to the standard spherical basis in Table I. In Figs. 4 and 5, we have visualized the mass distributions in the 2D BF and

TABLE I. Conversion from the our basis to the standard spherical basis.

Quantization axis n	$ s_n = 1\rangle$	$ s_n = 0\rangle$	$ s_n = -1\rangle$
x -axis (transversal)	$\frac{1}{\sqrt{2}}(z\rangle - i y\rangle)$	$- x\rangle$	$-\frac{1}{\sqrt{2}}(z\rangle + i y\rangle)$
y -axis (transversal)	$\frac{1}{\sqrt{2}}(x\rangle + i z\rangle)$	$-i y\rangle$	$\frac{1}{\sqrt{2}}(x\rangle - i z\rangle)$
z -axis (longitudinal)	$-\frac{1}{\sqrt{2}}(x\rangle + i y\rangle)$	$ z\rangle$	$\frac{1}{\sqrt{2}}(x\rangle - i y\rangle)$

2D IMF, respectively, taking a specific polarization of the spin-1 particle. We show here how to compute the mass distributions when the polarization is fixed. In Eq. (B1), the mass distribution in the 2D BF is written as

$$T_{\text{EF}}^{00}(\mathbf{x}_\perp, 0, \lambda', \lambda) = \delta_{3\lambda} \delta_{\lambda'3} \varepsilon_{(0,0)}^{(2D)}(\mathbf{x}_\perp) + \delta_{\sigma'\sigma} \varepsilon_{(0,1)}^{(2D)}(\mathbf{x}_\perp) + \hat{Q}_{\lambda'\lambda}^{ij} X_2^{ij}(\theta) \varepsilon_2^{(2D)}(\mathbf{x}_\perp), \tag{B1}$$

where λ and λ' run over x , y , and z whereas σ and σ' lie in the 2D EF, i.e. they take either x or y . We shall use θ instead of θ_{x_\perp} for convenience. When the spin-1 particle is polarized along the z -axis (s_z) and s_z is explicitly given, we have to get the matrix elements of T^{00} as follows:

$$\begin{aligned}
s_z = 0 &\rightarrow \langle z | \hat{O} | z \rangle \\
s_z = 1 &\rightarrow \frac{1}{2} \left[\langle x | \hat{O} | x \rangle + \langle y | \hat{O} | y \rangle + i \langle x | \hat{O} | y \rangle - i \langle y | \hat{O} | x \rangle \right] \\
s_z = -1 &\rightarrow \frac{1}{2} \left[\langle x | \hat{O} | x \rangle + \langle y | \hat{O} | y \rangle - i \langle x | \hat{O} | y \rangle + i \langle y | \hat{O} | x \rangle \right]. \tag{B2}
\end{aligned}$$

On the other hand, when it is polarized along the x -axis (s_x), we find the matrix elements as

$$\begin{aligned}
s_x = 0 &\rightarrow \langle x | \hat{O} | x \rangle \\
s_x = 1 &\rightarrow \frac{1}{2} \left[\langle z | \hat{O} | z \rangle + \langle y | \hat{O} | y \rangle - i \langle z | \hat{O} | y \rangle + i \langle y | \hat{O} | z \rangle \right] \\
s_x = -1 &\rightarrow \frac{1}{2} \left[\langle z | \hat{O} | z \rangle + \langle y | \hat{O} | y \rangle + i \langle z | \hat{O} | y \rangle - i \langle y | \hat{O} | z \rangle \right]. \tag{B3}
\end{aligned}$$

With the spin-1 particle polarized along the y -axis (s_y), we get

$$\begin{aligned} s_y = 0 &\rightarrow \langle y|\hat{O}|y\rangle \\ s_y = 1 &\rightarrow \frac{1}{2} \left[\langle x|\hat{O}|x\rangle + \langle z|\hat{O}|z\rangle + i\langle x|\hat{O}|z\rangle - i\langle z|\hat{O}|x\rangle \right] \\ s_y = -1 &\rightarrow \frac{1}{2} \left[\langle x|\hat{O}|x\rangle + \langle z|\hat{O}|z\rangle - i\langle x|\hat{O}|z\rangle + i\langle z|\hat{O}|x\rangle \right], \end{aligned} \quad (\text{B4})$$

where \hat{O} is a multipole operator. In the Cartesian basis, the matrix representations of the quadrupole operator $\langle \lambda'|\hat{Q}^{ij}|\lambda\rangle := \hat{Q}_{\lambda'\lambda}^{ij}$ are given by

$$\hat{Q}_{\lambda'\lambda}^{xx} = \begin{pmatrix} \lambda\backslash\lambda' & x & y & z \\ x & -\frac{2}{3} & 0 & 0 \\ y & 0 & \frac{1}{3} & 0 \\ z & 0 & 0 & \frac{1}{3} \end{pmatrix}, \quad \hat{Q}_{\lambda'\lambda}^{yy} = \begin{pmatrix} \lambda\backslash\lambda' & x & y & z \\ x & \frac{1}{3} & 0 & 0 \\ y & 0 & -\frac{2}{3} & 0 \\ z & 0 & 0 & \frac{1}{3} \end{pmatrix}, \quad \hat{Q}_{\lambda'\lambda}^{zz} = \begin{pmatrix} \lambda\backslash\lambda' & x & y & z \\ x & \frac{1}{3} & 0 & 0 \\ y & 0 & \frac{1}{3} & 0 \\ z & 0 & 0 & -\frac{2}{3} \end{pmatrix} \quad (\text{B5})$$

$$\hat{Q}_{\lambda'\lambda}^{xy} = \begin{pmatrix} \lambda\backslash\lambda' & x & y & z \\ x & 0 & -\frac{1}{2} & 0 \\ y & -\frac{1}{2} & 0 & 0 \\ z & 0 & 0 & 0 \end{pmatrix}, \quad \hat{Q}_{\lambda'\lambda}^{xz} = \begin{pmatrix} \lambda\backslash\lambda' & x & y & z \\ x & 0 & 0 & -\frac{1}{2} \\ y & 0 & 0 & 0 \\ z & -\frac{1}{2} & 0 & 0 \end{pmatrix}, \quad \hat{Q}_{\lambda'\lambda}^{yz} = \begin{pmatrix} \lambda\backslash\lambda' & x & y & z \\ x & 0 & 0 & 0 \\ y & 0 & 0 & -\frac{1}{2} \\ z & 0 & -\frac{1}{2} & 0 \end{pmatrix}. \quad (\text{B6})$$

Having contracted the $i, j = 1, 2$ indices to the x_{\perp}^i and x_{\perp}^j , we have the following expressions:

$$\begin{aligned} \hat{Q}_{\lambda'\lambda}^{ij} \hat{x}_{\perp}^i \hat{x}_{\perp}^j &:= \hat{Q}_{\lambda'\lambda}^{rr} = \begin{pmatrix} \frac{1}{6}(-1 - 3 \cos 2\theta) & -\cos \theta \sin \theta & 0 \\ -\cos \theta \sin \theta & \frac{1}{6}(-1 + 3 \cos 2\theta) & 0 \\ 0 & 0 & \frac{1}{3} \end{pmatrix}, \\ \hat{Q}_{\lambda'\lambda}^{ij} \hat{\theta}^i \hat{x}_{\perp}^j &= \hat{Q}_{\lambda'\lambda}^{\theta r} = \begin{pmatrix} \cos \theta \sin \theta & -\frac{1}{2} \cos 2\theta & 0 \\ -\frac{1}{2} \cos 2\theta & -\cos \theta \sin \theta & 0 \\ 0 & 0 & \frac{1}{3} \end{pmatrix}, \\ \hat{Q}_{\lambda'\lambda}^{ij} \hat{\theta}^i \hat{\theta}^j &= \hat{Q}_{\lambda'\lambda}^{\theta\theta} = \begin{pmatrix} \frac{1}{6}(-1 + 3 \cos 2\theta) & \cos \theta \sin \theta & 0 \\ \cos \theta \sin \theta & \frac{1}{6}(-1 - 3 \cos 2\theta) & 0 \\ 0 & 0 & \frac{1}{3} \end{pmatrix}. \end{aligned} \quad (\text{B7})$$

If the spin-1 particle is polarized with $s_z = 0$, then there is no θ dependence. So, the mass distribution contains only the scalar one $\varepsilon_{(0,0)}^{(2D)}(x_{\perp})$:

$$T_{\text{EF}}^{00}(\mathbf{x}_{\perp}, 0, \lambda', \lambda) = \delta_{zz} \delta_{zz} \varepsilon_{(0,0)}^{(2D)}(x_{\perp}) + (\hat{Q}_{zz}^{rr} - \frac{1}{2} \hat{Q}_{zz}^{ii}) \varepsilon_2^{(2D)}(x_{\perp}) = \varepsilon_{(0,0)}^{(2D)}(x_{\perp}). \quad (\text{B8})$$

If, however, it is polarized with $s_z = 1$, then we obtain T^{00} as

$$\begin{aligned} T_{\text{EF}}^{00}(\mathbf{x}_{\perp}, 0, \lambda', \lambda) &= \delta_{\sigma'\sigma} \varepsilon_{(0,1)}^{(2D)}(x_{\perp}) + (\hat{Q}_{s'_z=1, s_z=1}^{rr} - \frac{1}{2} \hat{Q}_{s'_z=1, s_z=1}^{ii}) \varepsilon_2^{(2D)}(x_{\perp}) \\ &= \frac{1}{2} (\delta_{xx} + \delta_{yy}) \varepsilon_{(0,1)}^{(2D)}(x_{\perp}) + (\hat{Q}_{s'_z=1, s_z=1}^{rr} - \frac{1}{2} \hat{Q}_{s'_z=1, s_z=1}^{ii}) \varepsilon_2^{(2D)}(x_{\perp}) \\ &= \varepsilon_{(0,1)}^{(2D)}(x_{\perp}). \end{aligned} \quad (\text{B9})$$

Note that we have the following algebra:

$$\begin{aligned} \hat{Q}_{s'_z=1, s_z=1}^{rr} - \frac{1}{2} \hat{Q}_{s'_z=1, s_z=1}^{ii} &= 0, \\ \hat{Q}_{s'_z=0, s_z=0}^{rr} - \frac{1}{2} \hat{Q}_{s'_z=0, s_z=0}^{ii} &= 0, \\ \hat{Q}_{s'_x=0, s_x=0}^{rr} - \frac{1}{2} \hat{Q}_{s'_x=0, s_x=0}^{ii} &= -\frac{1}{2} \cos 2\theta, \\ \hat{Q}_{s'_x=1, s_x=1}^{rr} - \frac{1}{2} \hat{Q}_{s'_x=1, s_x=1}^{ii} &= \frac{1}{4} \cos 2\theta. \end{aligned} \quad (\text{B10})$$

Thus, the quadrupole contribution vanishes when the spin-1 particle is polarized along the z -axis. However, if it is transversely polarized with $s_x = 0$, we get the contribution from the quadrupole term

$$T_{\text{EF}}^{00}(\mathbf{x}_\perp, 0, \lambda', \lambda) = \delta_{xx} \varepsilon_{(0,1)}^{(2\text{D})}(x_\perp) + (\hat{Q}_{xx}^{rr} - \frac{1}{2} \hat{Q}_{xx}^{ii}) \varepsilon_2^{(2\text{D})}(x_\perp) = \varepsilon_{(0,1)}^{(2\text{D})}(x_\perp) - \frac{1}{2} \cos 2\theta \varepsilon_2^{(2\text{D})}(x_\perp). \quad (\text{B11})$$

When the spin-1 particle is polarized with $s_x = 1$, we obtain the following mass distribution

$$\begin{aligned} T_{\text{EF}}^{00}(\mathbf{x}_\perp, 0, \lambda', \lambda) &= \frac{1}{2} \delta_{zz} \delta_{zz} \varepsilon_{(0,0)}^{(2\text{D})}(x_\perp) + \frac{1}{2} \delta_{yy} \varepsilon_{(0,1)}^{(2\text{D})}(x_\perp) + (\hat{Q}_{s'_x=1, s_x=1}^{rr} - \frac{1}{2} \hat{Q}_{s'_x=1, s_x=1}^{ii}) \varepsilon_2^{(2\text{D})}(x_\perp) \\ &= \frac{1}{2} \varepsilon_{(0,0)}^{(2\text{D})}(x_\perp) + \frac{1}{2} \varepsilon_{(0,1)}^{(2\text{D})}(x_\perp) + \frac{1}{4} \cos 2\theta \varepsilon_2^{(2\text{D})}(x_\perp). \end{aligned} \quad (\text{B12})$$

We can carry out a similar algebra to obtain the mass distributions in the 2D IMF. To obtain the force fields in the 2D BF and 2D IMF, we can perform a similar calculation.

In the IMF, we have additional dipole contribution, which is induced by the Lorentz boost.

$$\sim \epsilon^{3jk} \hat{S}_{\lambda'\lambda}^j X_1^k. \quad (\text{B13})$$

In the Cartesian basis, the matrix representations of the spin operator $\langle \lambda' | \hat{S}^i | \lambda \rangle := \hat{S}_{\lambda'\lambda}^i$ are given by

$$\hat{S}_{\lambda'\lambda}^x = \begin{pmatrix} \lambda \backslash \lambda' & x & y & z \\ x & 0 & 0 & 0 \\ y & 0 & 0 & -i \\ z & 0 & i & 0 \end{pmatrix}, \quad \hat{S}_{\lambda'\lambda}^y = \begin{pmatrix} \lambda \backslash \lambda' & x & y & z \\ x & 0 & 0 & i \\ y & 0 & 0 & 0 \\ z & -i & 0 & 0 \end{pmatrix}, \quad \hat{S}_{\lambda'\lambda}^z = \begin{pmatrix} \lambda \backslash \lambda' & x & y & z \\ x & 0 & -i & 0 \\ y & i & 0 & 0 \\ z & 0 & 0 & 0 \end{pmatrix} \quad (\text{B14})$$

Having contracted the $j, k = 1, 2$ indices to the $\epsilon^{3jk} X_1^k$, we have the following expressions:

$$\epsilon^{3jk} \hat{S}_{\lambda'\lambda}^j X_1^k = \begin{pmatrix} \lambda \backslash \lambda' & x & y & z \\ x & 0 & 0 & -\cos \theta \\ y & 0 & 0 & -i \sin \theta \\ z & i \cos \theta & i \sin \theta & 0 \end{pmatrix}, \quad (\text{B15})$$

Note that the diagonal components vanish, and the transverse states $|x, y\rangle$ should be mixed with the $|z\rangle$, so that we have a finite contribution to the mass distributions. Since there is no mixture of the them, the dipole contribution vanishes when the spin-1 particle is polarized along the z -axis.

Similarly, if it is transversely polarized with $s_x = 0$, we still have null contribution from the induced dipole term. However, if it is polarized with $s_x = \pm 1$ we then have finite contribution:

$$\begin{aligned} \epsilon^{3jk} \hat{S}_{\lambda'\lambda}^j X_1^k &= \sin \theta \quad (s_x = 1) \\ \epsilon^{3jk} \hat{S}_{\lambda'\lambda}^j X_1^k &= 0 \quad (s_x = 0) \\ \epsilon^{3jk} \hat{S}_{\lambda'\lambda}^j X_1^k &= -\sin \theta \quad (s_x = -1) \\ \epsilon^{3jk} \hat{S}_{\lambda'\lambda}^j X_1^k &= \cos \theta \quad (s_y = 1) \\ \epsilon^{3jk} \hat{S}_{\lambda'\lambda}^j X_1^k &= 0 \quad (s_y = 0) \\ \epsilon^{3jk} \hat{S}_{\lambda'\lambda}^j X_1^k &= -\cos \theta \quad (s_y = -1) \end{aligned} \quad (\text{B16})$$

One can clearly see in Fig. 5 that the dipole contributes to the mass distribution only with $s_x = 1$. In the other figures, such contributions vanish.

Appendix C: Explicit calculation of the mechanical distributions

In this Appendix, we show explicitly the mechanical distributions for a spin-1 particle. When we have $s_z = 0$, the matrix elements of the dipole and quadrupole operators are obtained as

$$\hat{Q}_{s'_z=0, s_z=0}^{rr} = \frac{1}{3}, \quad \hat{Q}_{s'_z=0, s_z=0}^{\theta\theta} = \frac{1}{3}, \quad \hat{Q}_{s'_z=0, s_z=0}^{\theta r} = 0, \quad \epsilon^{lm3} \hat{S}_{s'_z=0, s_z=0}^l X_1^m(\theta) = 0, \quad \epsilon^{lm3} \hat{S}_{s'_z=0, s_z=0}^l \hat{\theta}_1^m(\theta) = 0. \quad (\text{C1})$$

Thus, we can show that the quadrupole pattern of the distribution vanishes when the spin-1 particle is polarized along the z -axis ($s_z = 0$):

$$\begin{aligned}
\frac{dF_r}{dS_r} &= \left[\left(p_{(0,0)}^{\text{IMF}} + \frac{1}{2} s_{(0,0)}^{\text{IMF}} \right) + \frac{2}{3} \left(2p_2^{\text{IMF}} + s_2^{\text{IMF}} + \frac{1}{m^2} \left[-\frac{s_3^{\text{IMF}'}}{2x_\perp} - \frac{p_3^{\text{IMF}'}}{x_\perp} + \frac{2s_3^{\text{IMF}}}{x_\perp^2} \right] \right) \right] \\
&\quad + \frac{1}{3} \frac{1}{m^2} \left[-p_3^{\text{IMF}''} + \frac{p_3^{\text{IMF}'}}{x_\perp} - \frac{s_3^{\text{IMF}''}}{2} + \frac{s_3^{\text{IMF}'}}{2x_\perp} - \frac{2s_3^{\text{IMF}}}{x_\perp^2} \right], \\
\frac{dF_r}{dS_\theta} &= \frac{dF_\theta}{dS_r} = 0, \\
\frac{dF_\theta}{dS_\theta} &= \left[\left(p_{(0,0)}^{\text{IMF}} - \frac{1}{2} s_{(0,0)}^{\text{IMF}} \right) + \frac{2}{3} \left(2p_2^{\text{IMF}} + s_2^{\text{IMF}} + \frac{1}{m^2} \left[\frac{s_3^{\text{IMF}'}}{2x_\perp} - \frac{p_3^{\text{IMF}'}}{x_\perp} \right] \right) \right] \delta_{\lambda'3} \delta_{3\lambda} \\
&\quad + \frac{1}{3} \left(-2s_2^{\text{IMF}} + \frac{1}{m^2} \left[-p_3^{\text{IMF}''} + \frac{p_3^{\text{IMF}'}}{x_\perp} + \frac{s_3^{\text{IMF}''}}{2} - \frac{s_3^{\text{IMF}'}}{2x_\perp} \right] \right) + \frac{1}{3} \left[-2s_2^{\text{IMF}} - \frac{2}{m^2} \frac{s_3^{\text{IMF}}}{x_\perp^2} \right]. \tag{C2}
\end{aligned}$$

Since there is no θ dependence on $dF_{r,\theta}/dS_{r,\theta}$, the visualized forces looks like the unpolarized nucleon force distributions, except for the strengths of them.

When the spin-1 particle is polarized along the z -axis with $s_z = 1$, we find the matrix elements of the dipole and quadrupole operators as follows:

$$\begin{aligned}
\hat{Q}_{s'_z=1, s_z=1}^{rr} &= -\frac{1}{6}, \quad \hat{Q}_{s'_z=1, s_z=1}^{\theta\theta} = -\frac{1}{6}, \quad \hat{Q}_{s'_z=1, s_z=1}^{\theta r} = 0, \\
\epsilon^{lm3} \hat{S}_{s'_z=1, s_z=1}^l X_1^m(\theta) &= 0, \quad \epsilon^{lm3} \hat{S}_{s'_z=1, s_z=1}^l \hat{\theta}_1^m(\theta) = 0. \tag{C3}
\end{aligned}$$

So, the quadrupole pattern of the distribution again vanishes when the spin-1 particle is polarized along the z -axis with $s_z = 1$:

$$\begin{aligned}
\frac{dF_r}{dS_r} &= \left[\left(p_{(0,1)}^{\text{IMF}} + \frac{1}{2} s_{(0,1)}^{\text{IMF}} \right) - \frac{1}{3} \left(2p_2^{\text{IMF}} + s_2^{\text{IMF}} + \frac{1}{m^2} \left[-\frac{s_3^{\text{IMF}'}}{2x_\perp} - \frac{p_3^{\text{IMF}'}}{x_\perp} + \frac{2s_3^{\text{IMF}}}{x_\perp^2} \right] \right) \right] \\
&\quad - \frac{1}{6} \frac{1}{m^2} \left[-p_3^{\text{IMF}''} + \frac{p_3^{\text{IMF}'}}{x_\perp} - \frac{s_3^{\text{IMF}''}}{2} + \frac{s_3^{\text{IMF}'}}{2x_\perp} - \frac{2s_3^{\text{IMF}}}{x_\perp^2} \right], \\
\frac{dF_r}{dS_\theta} &= \frac{dF_\theta}{dS_r} = 0, \\
\frac{dF_\theta}{dS_\theta} &= \left[\left(p_{(0,1)}^{\text{IMF}} - \frac{1}{2} s_{(0,1)}^{\text{IMF}} \right) - \frac{1}{3} \left(2p_2^{\text{IMF}} + s_2^{\text{IMF}} + \frac{1}{m^2} \left[\frac{s_3^{\text{IMF}'}}{2x_\perp} - \frac{p_3^{\text{IMF}'}}{x_\perp} \right] \right) \right] \\
&\quad - \frac{1}{6} \left(-2s_2^{\text{IMF}} + \frac{1}{m^2} \left[-p_3^{\text{IMF}''} + \frac{p_3^{\text{IMF}'}}{x_\perp} + \frac{s_3^{\text{IMF}''}}{2} - \frac{s_3^{\text{IMF}'}}{2x_\perp} \right] \right) - \frac{1}{6} \left[-2s_2^{\text{IMF}} - \frac{2}{m^2} \frac{s_3^{\text{IMF}}}{x_\perp^2} \right]. \tag{C4}
\end{aligned}$$

Note that for $s_z = 1$ they are still independent of θ , which means that they are spherically symmetric.

When the spin-1 particle is transversely polarized along x -axis with $s_x = 0$, θ dependence of $dF_{r,\theta}/dS_{r,\theta}$ emerges. In this case, the matrix elements of the dipole and quadrupole operators are derived as

$$\begin{aligned}
\hat{Q}_{s'_x=0, s_x=0}^{rr} &= -\frac{1}{6}(1 + 3 \cos 2\theta), \quad \hat{Q}_{s'_x=0, s_x=0}^{\theta\theta} = -\frac{1}{6}(1 - 3 \cos 2\theta), \quad \hat{Q}_{s'_x=0, s_x=0}^{\theta r} = \cos \theta \sin \theta, \\
\epsilon^{lm3} \hat{S}_{s'_x=0, s_x=0}^l X_1^m(\theta) &= 0, \quad \epsilon^{lm3} \hat{S}_{s'_x=0, s_x=0}^l \hat{\theta}_1^m(\theta) = 0. \tag{C5}
\end{aligned}$$

Thus, the strong force fields can be directly obtained as

$$\begin{aligned}
\frac{dF_r}{dS_r} &= \left[\left(p_{(0,1)}^{\text{IMF}} + \frac{1}{2} s_{(0,1)}^{\text{IMF}} \right) - \frac{1}{3} \left(2p_2^{\text{IMF}} + s_2^{\text{IMF}} + \frac{1}{m^2} \left[-\frac{s_3^{\text{IMF}'}}{2x_\perp} - \frac{p_3^{\text{IMF}'}}{x_\perp} + \frac{2s_3^{\text{IMF}}}{x_\perp^2} \right] \right) \right] \\
&\quad - \frac{1}{6} (1 + 3 \cos 2\theta) \frac{1}{m^2} \left[-p_3^{\text{IMF}''} + \frac{p_3^{\text{IMF}'}}{x_\perp} - \frac{s_3^{\text{IMF}''}}{2} + \frac{s_3^{\text{IMF}'}}{2x_\perp} - \frac{2s_3^{\text{IMF}}}{x_\perp^2} \right], \\
\frac{dF_r}{dS_\theta} &= \frac{dF_\theta}{dS_r} = \cos \theta \sin \theta \frac{1}{m^2} \left[-\frac{2s_3^{\text{IMF}'}}{x_\perp} + \frac{2s_3^{\text{IMF}}}{x_\perp^2} \right], \\
\frac{dF_\theta}{dS_\theta} &= \left[\left(p_{(0,1)}^{\text{IMF}} - \frac{1}{2} s_{(0,1)}^{\text{IMF}} \right) - \frac{1}{3} \left(2p_2^{\text{IMF}} + s_2^{\text{IMF}} + \frac{1}{m^2} \left[\frac{s_3^{\text{IMF}'}}{2x_\perp} - \frac{p_3^{\text{IMF}'}}{x_\perp} \right] \right) \right] \\
&\quad - \frac{1}{6} (1 + 3 \cos 2\theta) \left(-2s_2^{\text{IMF}} + \frac{1}{m^2} \left[-p_3^{\text{IMF}''} + \frac{p_3^{\text{IMF}'}}{x_\perp} + \frac{s_3^{\text{IMF}''}}{2} - \frac{s_3^{\text{IMF}'}}{2x_\perp} \right] \right) \\
&\quad - \frac{1}{6} (1 - 3 \cos 2\theta) \left[-2s_2^{\text{IMF}} - \frac{2}{m^2} \frac{s_3^{\text{IMF}}}{x_\perp^2} \right]. \tag{C6}
\end{aligned}$$

While all the dipole contribution still found to be zero, the qudrupole structure brings about the deformation of the strong force distributions.

The most interesting case arises when the spin-1 particle is polarized along the x -axis with $s_x = 1$. The matrix elements of $\hat{Q}_{s'_x=1, s_x=1}$ and $\hat{S}_{s'_x=1, s_x=1}$ are given by

$$\begin{aligned}
\hat{Q}_{s'_x=1, s_x=1}^{rr} &= \frac{1}{12} (1 + 3 \cos 2\theta), \quad \hat{Q}_{s'_x=1, s_x=1}^{\theta\theta} = \frac{1}{12} (1 - 3 \cos 2\theta), \quad \hat{Q}_{s'_x=1, s_x=1}^{\theta r} = -\frac{1}{2} \cos \theta \sin \theta, \\
\epsilon^{lm3} \hat{S}_{s'_x=1, s_x=1}^l X_1^m(\theta) &= \sin \theta, \quad \epsilon^{lm3} \hat{S}_{s'_x=1, s_x=1}^l \hat{\theta}_1^m(\theta) = \cos \theta. \tag{C7}
\end{aligned}$$

Using these results, we can show that all the dipole and quadrupole contributions to the strong force fields emerge as follows:

$$\begin{aligned}
\frac{dF_r}{dS_r} &= \frac{1}{2} \left[\left(p_{(0,1)}^{\text{IMF}} + \frac{1}{2} s_{(0,1)}^{\text{IMF}} \right) - \frac{1}{3} \left(2p_2^{\text{IMF}} + s_2^{\text{IMF}} + \frac{1}{m^2} \left[-\frac{s_3^{\text{IMF}'}}{2x_\perp} - \frac{p_3^{\text{IMF}'}}{x_\perp} + \frac{2s_3^{\text{IMF}}}{x_\perp^2} \right] \right) \right] \\
&\quad + \frac{1}{2} \left[\left(p_{(0,0)}^{\text{IMF}} + \frac{1}{2} s_{(0,0)}^{\text{IMF}} \right) + \frac{2}{3} \left(2p_2^{\text{IMF}} + s_2^{\text{IMF}} + \frac{1}{m^2} \left[-\frac{s_3^{\text{IMF}'}}{2x_\perp} - \frac{p_3^{\text{IMF}'}}{x_\perp} + \frac{2s_3^{\text{IMF}}}{x_\perp^2} \right] \right) \right] \\
&\quad + \frac{1}{12} (1 + 3 \cos 2\theta) \frac{1}{m^2} \left[-p_3^{\text{IMF}''} + \frac{p_3^{\text{IMF}'}}{x_\perp} - \frac{s_3^{\text{IMF}''}}{2} + \frac{s_3^{\text{IMF}'}}{2x_\perp} - \frac{2s_3^{\text{IMF}}}{x_\perp^2} \right] - \sin \theta \frac{1}{m} [2p_1^{\text{IMF}'} + s_1^{\text{IMF}'}], \\
\frac{dF_r}{dS_\theta} &= \frac{dF_\theta}{dS_r} = -\frac{1}{2} \cos \theta \sin \theta \frac{1}{m^2} \left[-\frac{2s_3^{\text{IMF}'}}{x_\perp} + \frac{2s_3^{\text{IMF}}}{x_\perp^2} \right] - \frac{2}{m} \cos \theta \frac{s_1^{\text{IMF}}}{x_\perp}, \\
\frac{dF_\theta}{dS_\theta} &= \frac{1}{2} \left[\left(p_{(0,1)}^{\text{IMF}} - \frac{1}{2} s_{(0,1)}^{\text{IMF}} \right) - \frac{1}{3} \left(2p_2^{\text{IMF}} + s_2^{\text{IMF}} + \frac{1}{m^2} \left[\frac{s_3^{\text{IMF}'}}{2x_\perp} - \frac{p_3^{\text{IMF}'}}{x_\perp} \right] \right) \right] \\
&\quad + \frac{1}{2} \left[\left(p_{(0,0)}^{\text{IMF}} - \frac{1}{2} s_{(0,0)}^{\text{IMF}} \right) + \frac{2}{3} \left(2p_2^{\text{IMF}} + s_2^{\text{IMF}} + \frac{1}{m^2} \left[\frac{s_3^{\text{IMF}'}}{2x_\perp} - \frac{p_3^{\text{IMF}'}}{x_\perp} \right] \right) \right] \\
&\quad + \frac{1}{12} (1 + 3 \cos 2\theta) \left(-2s_2^{\text{IMF}} + \frac{1}{m^2} \left[-p_3^{\text{IMF}''} + \frac{p_3^{\text{IMF}'}}{x_\perp} + \frac{s_3^{\text{IMF}''}}{2} - \frac{s_3^{\text{IMF}'}}{2x_\perp} \right] \right) \\
&\quad + \frac{1}{12} (1 - 3 \cos 2\theta) \left[-2s_2^{\text{IMF}} - \frac{2}{m^2} \frac{s_3^{\text{IMF}}}{x_\perp^2} \right] - \sin \theta \frac{1}{m} [2p_1^{\text{IMF}'} - s_1^{\text{IMF}'}]. \tag{C8}
\end{aligned}$$

-
- [1] M. V. Polyakov and P. Schweitzer, Int. J. Mod. Phys. A **33**, no.26, 1830025 (2018).
[2] D. Müller, D. Robaschik, B. Geyer, F. M. Dittes and J. Hořejši, Fortsch. Phys. **42**, 101-141 (1994).
[3] X. D. Ji, Phys. Rev. Lett. **78**, 610-613 (1997).
[4] A. V. Radyushkin, Phys. Lett. B **380**, 417-425 (1996).
[5] A. V. Radyushkin, Phys. Lett. B **385**, 333-342 (1996).
[6] X. D. Ji, Phys. Rev. D **55**, 7114-7125 (1997).

- [7] I. Y. Kobzarev and L. B. Okun, *Zh. Eksp. Teor. Fiz.* **43**, 1904-1909 (1962).
- [8] H. Pagels, *Phys. Rev.* **144**, 1250-1260 (1966).
- [9] M. Burkardt, *Phys. Rev. D* **62**, 071503 (2000) [erratum: *Phys. Rev. D* **66**, 119903 (2002)].
- [10] J. P. Ralston and B. Pire, *Phys. Rev. D* **66**, 111501 (2002).
- [11] M. Burkardt, *Int. J. Mod. Phys. A* **18**, 173-208 (2003).
- [12] G. A. Miller, *Phys. Rev. Lett.* **99**, 112001 (2007).
- [13] C. Lorcé and P. Wang, *Phys. Rev. D* **105**, no.9, 096032 (2022).
- [14] J. Y. Kim, *Phys. Rev. D* **106**, no.1, 014022 (2022).
- [15] C. E. Carlson and M. Vanderhaeghen, *Eur. Phys. J. A* **41**, 1-5 (2009).
- [16] B. D. Sun and Y. B. Dong, *Chin. Phys. C* **42**, no.6, 063104 (2018).
- [17] D. A. Pefkou, D. C. Hackett and P. E. Shanahan, *Phys. Rev. D* **105**, no.5, 054509 (2022).
- [18] M. V. Polyakov and P. Schweitzer, *PoS SPIN2018*, 066 (2019).
- [19] J. Y. Kim and B. D. Sun, *Eur. Phys. J. C* **81**, no.1, 85 (2021).
- [20] D. R. Yennie, M. M. Levy, and D. G. Ravenhall, *Rev. Mod. Phys.* **29**, 144 (1957).
- [21] M. V. Polyakov, *Phys. Lett. B* **555**, 57-62 (2003).
- [22] K. Goetze, J. Grabis, J. Ossmann, M. V. Polyakov, P. Schweitzer, A. Silva and D. Urbano, *Phys. Rev. D* **75**, 094021 (2007).
- [23] R. L. Jaffe, *Phys. Rev. D* **103**, no.1, 016017 (2021).
- [24] A. V. Belitsky and A. V. Radyushkin, *Phys. Rept.* **418**, 1-387 (2005).
- [25] C. Lorcé, *Phys. Rev. Lett.* **125**, no.23, 232002 (2020).
- [26] J. Y. Panteleeva and M. V. Polyakov, *Phys. Rev. D* **104**, no.1, 014008 (2021).
- [27] J. Y. Kim and H.-Ch. Kim, *Phys. Rev. D* **104**, no.7, 074019 (2021).
- [28] J. Y. Kim and H.-Ch. Kim, *Phys. Rev. D* **104**, no.7, 074003 (2021).
- [29] M. V. Polyakov, *Phys. Lett. B* **659**, 542 (2008).
- [30] A. M. Moiseeva and M. V. Polyakov, *Nucl. Phys. B* **832**, 241 (2010).
- [31] E. Epelbaum, J. Gegelia, N. Lange, U. G. Meißner and M. V. Polyakov, *Phys. Rev. Lett.* **129**, no.1, 012001 (2022).
- [32] J. Y. Panteleeva, E. Epelbaum, J. Gegelia and U. G. Meißner, [arXiv:2205.15061 [hep-ph]].
- [33] A. Freese and G. A. Miller, *Phys. Rev. D* **105**, no.1, 014003 (2022).
- [34] B. D. Sun and Y. B. Dong, *Phys. Rev. D* **101**, no.9, 096008 (2020).
- [35] F. J. Belinfante, *Physica* **6**, 887 (1939).
- [36] W. Pauli and F. J. Belinfante, *Physica* **7**, 177 (1940).
- [37] C. G. Callan, Jr., S. R. Coleman and R. Jackiw, *Annals Phys.* **59**, 42 (1970).
- [38] L. E. Parker and D. Toms, "Quantum Field Theory in Curved Spacetime: Quantized Field and Gravity," (Cambridge University Press, Cambridge, UK, 2009).
- [39] S. Cotogno, C. Lorcé, P. Lowdon and M. Morales, *Phys. Rev. D* **101**, no.5, 056016 (2020).
- [40] W. Cosyn, S. Cotogno, A. Freese and C. Lorcé, *Eur. Phys. J. C* **79**, no.6, 476 (2019).
- [41] M. V. Polyakov and B. D. Sun, *Phys. Rev. D* **100**, no.3, 036003 (2019).
- [42] W. N. Polyzou, W. Glöckle and H. Witala, *Few Body Syst.* **54**, 1667-1704 (2013).
- [43] C. Lorcé and P. Lowdon, *Eur. Phys. J. C* **80**, no.3, 207 (2020).
- [44] C. Lorcé, H. Moutarde and A. P. Trawiński, *Eur. Phys. J. C* **79**, 89 (2019).
- [45] C. Alexandrou, T. Korzec, G. Koutsou, C. Lorce, J. W. Negele, V. Pascalutsa, A. Tsapalis and M. Vanderhaeghen, *Nucl. Phys. A* **825**, 115-144 (2009).
- [46] Harrison H. Barrett, *Progress in Optics*, **21**, 217 (1984).
- [47] R. N. Bracewell, *Australian Journal of Physics*, **9**, 198 (1956).
- [48] U. Leonhardt, "Measuring the quantum state of light, Cambridge Studies in Modern Optics", (Cambridge University Press, Cambridge, 1997).
- [49] F. Natterer, "The Mathematics of Computerized Tomography", (John Wiley & Sons, New York, 2001).
- [50] N.H. Abel, *J. Reine und Angew. Math.* **1**, 153 (1826).
- [51] J. Radon, *Berichte über die Verhandlungen der Königlich-Sächsischen Gesellschaft der Wissenschaften zu Leipzig, Mathematisch-Physische Klasse* **69**, 262 (1917).
- [52] C. Lorcé, L. Mantovani and B. Pasquini, *Phys. Lett. B* **776**, 38-47 (2018).
- [53] P. Schweitzer and K. Tezgin, *Phys. Lett. B* **796**, 47-51 (2019).
- [54] A. Freese and I. C. Cloët, *Phys. Rev. C* **100**, no.1, 015201 (2019).